

POLITECNICO DI TORINO

---

Department of Mechanical and Aerospace Engineering

Master degree course in Aerospace Engineering

Master Degree Thesis

**Evasion maneuvers with double lunar  
flyby for interplanetary missions**



**Supervisor**  
Lorenzo Casalino

**Candidate**  
Sebastiano BUGNO  
Matricola: 239257

---

ACADEMIC YEAR 2017-2018



# Acknowledgements

I would first like to thank my thesis advisor Professor Lorenzo Casalino of the Mechanics and Aerospace department (DIMEAS) at Politecnico of Turin. I owe him a special thanks, because he was always available for every problem or doubt about this thesis and his help it was essential for the success of the work.

In addition, I must express my very profound gratitude to my family for providing me with unfailing support and continuous encouragement throughout my years of study and for the moving to Turin. This accomplishment would not have been possible without them.

Thank you so much.



# Contents

<b>List of Figures</b>	III
<b>List of Tables</b>	V
<b>1 Introduction</b>	1
<b>2 Evasion maneuvers</b>	3
2.1 Short background on interplanetary missions . . . . .	3
2.2 Escape . . . . .	5
2.3 Flyby . . . . .	8
<b>3 Approximate analytical approach</b>	11
3.1 Introduction . . . . .	11
3.2 Trajectory analysis . . . . .	12
3.2.1 Moon to Escape . . . . .	13
3.2.2 Moon to Moon . . . . .	13
3.2.3 Perigee to Moon . . . . .	15
3.3 Calculations . . . . .	16
<b>4 Exact numerical solution</b>	19
4.1 Solution description . . . . .	19
4.2 Equations . . . . .	22
4.3 Perturbations . . . . .	23
4.3.1 Earth asphericity . . . . .	24
4.3.2 LuniSolar perturbation . . . . .	24
4.3.3 Solar radiation pressure . . . . .	26
<b>5 Approximate analytical approach results</b>	27
5.1 Features . . . . .	27
5.2 Case 0 (comparison between exact and approximated solution) . . . . .	29
5.3 Comparison between solutions with the same escape date . . . . .	34
5.4 Comparison between solutions with the same $V_\infty$ . . . . .	38

<b>6 Exact numerical solution results</b>	43
6.1 Comparison between solutions with the same escape date . . . . .	43
6.2 Comparison between solutions with the same $V_\infty$ . . . . .	49
6.3 Comparison between exact and approximated solutions . . . . .	54
6.3.1 Case 2 . . . . .	54
6.3.2 Case 4 . . . . .	57
6.3.3 Case 5 . . . . .	60
6.3.4 Case 6 . . . . .	63
<b>7 Conclusions</b>	67
<b>Glossary</b>	70
<b>Bibliography</b>	71

# List of Figures

2.1	Hohmann transfer from inner planet 1 to outer planet 2 [4] . . . . .	5
2.2	Departure of a spacecraft on a mission from an inner planet to an outer planet [4] . . . . .	6
2.3	Trailing-side planetary flyby [4] . . . . .	9
2.4	Changes in the inclination angle of the spacecraft orbit as result of gravity assist maneuver [8] . . . . .	10
3.1	Lunar escape trajectory with backflip . . . . .	11
3.2	Approximate analytical solution, 3D view . . . . .	12
3.3	Approximate analytical solution, XY plane . . . . .	14
3.4	Position at the flyby, with respect to the Moon . . . . .	17
4.1	Software solution output . . . . .	21
4.2	Schematic geometry of gravitational perturbations [5]. . . . .	25
5.1	Asteroid 2008 EV5's orbit (white) compared with the nearest planets, in the heliocentric reference system [14]. . . . .	28
5.2	3D visual of the asteroid and Earth orbit in the heliocentric reference system [14]. . . . .	29
5.3	Zoom on FB1, comparison between exact and approximate solution . . . . .	31
5.4	Zoom on FB2, comparison between exact and approximate solution . . . . .	32
5.5	Comparison between exact and approximate solution, Case 0 . . . . .	34
5.6	Comparison between solutions with the same escape date . . . . .	38
5.7	Comparison between solutions with the same $V_\infty$ . . . . .	42
6.1	Comparison between solutions as the $V_\infty$ varies, 3D view . . . . .	47
6.2	Comparison between solutions as the $V_\infty$ varies, XY view . . . . .	48
6.3	Comparison between solutions as the $V_\infty$ varies, YZ view . . . . .	48
6.4	Comparison between solutions as the escape date varies, 3D view . . . . .	52
6.5	Comparison between solutions as the escape date varies, XY view . . . . .	53
6.6	Comparison between solutions as the escape date varies, YZ view . . . . .	53
6.7	Comparison between exact and approximate solution, Case 2 . . . . .	57
6.8	Comparison between exact and approximate solution, Case 4 . . . . .	60
6.9	Comparison between exact and approximate solution, Case 5 . . . . .	63
6.10	Comparison between exact and approximate solution, Case 6 . . . . .	66



# List of Tables

5.1	Escape conditions . . . . .	28
5.2	Comparison of S/C-Moon positions at the two flybys between exact and approximate solution . . . . .	30
5.3	Comparison of relative positions at the two flybys between exact and approximate solution . . . . .	30
5.4	Comparison of S/C positions between exact and approximate solution . .	31
5.5	Time comparison between exact and approximate solution . . . . .	32
5.6	Comparison of orbital parameters between exact and approximate solution, part 1 . . . . .	32
5.7	Comparison of orbital parameters between exact and approximate solution, part 2 . . . . .	33
5.8	Energy comparison between exact and approximate solution . . . . .	33
5.9	Comparison of S/C-Moon positions at the two flybys between solutions with the same escape date . . . . .	34
5.10	Comparison of relative positions at the two flybys between solutions with the same escape date . . . . .	35
5.11	Comparison of S/C positions between solutions with the same escape date	36
5.12	Time comparison between solutions with the same escape date . . . . .	36
5.13	Comparison of orbital parameters between solutions with the same escape date, part 1 . . . . .	37
5.14	Comparison of orbital parameters between solutions with the same escape date, part 2 . . . . .	37
5.15	Energy comparison between solutions with the same escape date . . . . .	38
5.16	Comparison of S/C-Moon positions at the two flybys between solutions with the same $V_\infty$ . . . . .	39
5.17	Comparison of relative positions at the two flybys between solutions with the same $V_\infty$ . . . . .	39
5.18	Comparison of S/C positions between solutions with the same $V_\infty$ . . . .	40
5.19	Time comparison between solutions with the same $V_\infty$ . . . . .	40
5.20	Comparison of orbital parameters between solutions with the same $V_\infty$ , part 1 . . . . .	40
5.21	Comparison of orbital parameters between solutions with the same $V_\infty$ , part 2 . . . . .	41
5.22	Energy comparison between solutions with the same $V_\infty$ . . . . .	41

6.1	Mass and times as the $V_\infty$ varies . . . . .	43
6.2	Comparison of the periselenium radius at the 2 flybys . . . . .	44
6.3	Comparison of S/C-Moon positions at the two flybys . . . . .	44
6.4	Adimensional spherical coordinates of the S/C in points of particular interest as the $V_\infty$ varies . . . . .	45
6.5	Adimensional velocities of the S/C in points of particular interest as the $V_\infty$ varies . . . . .	46
6.6	Initial and final semi-axis and energy . . . . .	46
6.7	Mass and times as the date of escape varies . . . . .	49
6.8	Comparison of the periselenium radius at the 2 flybys . . . . .	49
6.9	Comparison of S/C-Moon positions at the two flybys . . . . .	50
6.10	Adimensional spherical coordinates of the S/C in points of particular interest as the date of escape varies . . . . .	51
6.11	Adimensional velocities of the S/C in points of particular interest as the date of escape varies . . . . .	51
6.12	Initial and final semi-axis and energy . . . . .	52
6.13	Comparison of S/C-Moon positions at the two flybys between exact and approximate solution . . . . .	54
6.14	Comparison of relative positions at the two flybys between exact and approximate solution . . . . .	54
6.15	Comparison of S/C positions between exact and approximate solution . . . . .	55
6.16	Time comparison between exact and approximate solution . . . . .	55
6.17	Comparison of orbital parameters between exact and approximate solution, part 1 . . . . .	55
6.18	Comparison of orbital parameters between exact and approximate solution, part 2 . . . . .	56
6.19	Energy comparison between exact and approximate solution . . . . .	56
6.20	Comparison of S/C-Moon positions at the two flybys between exact and approximate solution . . . . .	57
6.21	Comparison of relative positions at the two flybys between exact and approximate solution . . . . .	58
6.22	Comparison of S/C positions between exact and approximate solution . . . . .	58
6.23	Time comparison between exact and approximate solution . . . . .	58
6.24	Comparison of orbital parameters between exact and approximate solution, part 1 . . . . .	59
6.25	Comparison of orbital parameters between exact and approximate solution, part 2 . . . . .	59
6.26	Energy comparison between exact and approximate solution . . . . .	59
6.27	Comparison of S/C-Moon positions at the two flybys between exact and approximate solution . . . . .	60
6.28	Comparison of relative positions at the two flybys between exact and approximate solution . . . . .	61
6.29	Comparison of S/C positions between exact and approximate solution . . . . .	61
6.30	Time comparison between exact and approximate solution . . . . .	61

6.31	Comparison of orbital parameters between exact and approximate solution, part 1 . . . . .	62
6.32	Comparison of orbital parameters between exact and approximate solution, part 2 . . . . .	62
6.33	Energy comparison between exact and approximate solution . . . . .	62
6.34	Comparison of S/C-Moon positions at the two flybys between exact and approximate solution . . . . .	63
6.35	Comparison of relative positions at the two flybys between exact and ap- proximate solution . . . . .	64
6.36	Comparison of S/C positions between exact and approximate solution . .	64
6.37	Time comparison between exact and approximate solution . . . . .	64
6.38	Comparison of orbital parameters between exact and approximate solution, part 1 . . . . .	65
6.39	Comparison of orbital parameters between exact and approximate solution, part 2 . . . . .	65
6.40	Energy comparison between exact and approximate solution . . . . .	65



# Chapter 1

## Introduction

The purpose of this thesis is to describe and analyze a particular evasion maneuver with double lunar gravity assist (LGA) for interplanetary missions.

Lunar flybys are a means to free increase the hyperbolic escape energy (C3) of an escape maneuver for a modest increase in flight time.

Two approaches are applied:

- the first one is the approximate analytical approach;
- the second one gives the exact numerical solutions, because it takes into account all the main perturbations.

The approximate model, it is easier than the other one because it is based on simplifying assumptions such as: no gravitational influence of Sun and Moon on the spacecraft, no solar radiation pressure, no eccentricity of Moon's orbit (i.e. circular orbit), only Earth's gravitational pull. It is just a preliminary study but extremely helpful because it gives you a macro view of the whole trajectory. Even without going into too much detail, it provides all the most important information in terms of times, positions and velocities. In particular, the solution obtained from this model, is used as the attempt solution for the more detailed analysis.

Only short maneuvers, which should be less affected by solar perturbation are treated. For preliminary analysis of the interplanetary transfers, is usually adopted the patched conic approximation. The analysis of the heliocentric leg provides us the escape conditions.

In particular, our conditions refer to an Asteroid Redirect Mission (*ARM*), also known as the Asteroid Retrieval and Utilization (ARU) mission. It is a NASA space mission, proposed in 2013. An ARRM spacecraft (Asteroid Retrieval Robotic Mission) would rendezvous with a large near-Earth asteroid and use robotic arms in order to collect a multi-ton boulder from its surface and return it to a stable orbit around the Moon or the Earth. This Asteroid Redirect Mission is part of NASA's plan to advance the new technologies and spaceflight experience needed for a human mission to the Martian system in the 2030s.

All the solutions presented in the following chapters were obtained from these escape conditions as boundary conditions. At the boundary of the Earth's sphere of influence

(a concept that will be explained in detail in Chapter 2), are known the escape date, positions and escape velocity components of the spacecraft.

Solutions are then compared between the two different approaches and between the different escape conditions (Chapter 5 and 6). Escape conditions that differ either by the escape date or by the escape velocity.

Comparison between the two different models it is useful in order to verify the approximation committed by the simplest one, taking into consideration that this solution is obtained in less than 1 second (limited computational effort), compared to the much larger effort required to obtain the exact solution.

## Chapter 2

# Evasion maneuvers

In order to escape the gravitational pull of a planet, the spacecraft must travel a hyperbolic trajectory relative to the planet, arriving at its sphere of influence with a relative velocity  $\mathbf{V}_\infty$  (hyperbolic excess velocity) greater than zero. This is a simplification linked to our study. Actually, the truer statement is that S/C must arrive at an infinite distance with a non-zero relative velocity.

The sphere of influence (SOI) is a concept strictly related to the three-body problem. In general it involves: a planet  $p$  of mass  $m_p$ , the Sun  $s$  of mass  $m_s$  and a space vehicle  $v$  of mass  $m_v$  (negligible mass). It is simply a reasonable estimate of the distance beyond which Sun's gravitational attraction dominates that of a planet.

At this distance, our study ends, because beyond this distance it leads from geocentric escape leg to the heliocentric leg.

The radius of a planet's gravitational sphere of influence is calculated as the boundary where the error committed neglecting the Sun in the motion of the spacecraft with respect to the planet, is equal to neglecting the planet in the motion with respect to the Sun (i.e.

$$\frac{\text{perturbation of the Sun}}{\text{gravity of the Moon}} = \frac{\text{perturbation of the Moon}}{\text{gravity of the Sun}}).$$

For example, the SOI of the Earth, in the three-body problem with the Sun, is about 925000 km (generally, it is rounded to one million).

The same concepts are applied to the Earth - Moon system, where the sphere of influence of the latter is defined (about 60000 km).

### 2.1 Short background on interplanetary missions

An interplanetary mission is a trip through outer space involving more than one planet. For planetary missions, a spacecraft is launched from the Earth and accelerated to a velocity higher than the local escape velocity. The spacecraft will then recede from Earth along a hyperbolic trajectory.

The first successful interplanetary mission was that of the *US Mariner 2* spacecraft, which has flown by Venus at a minimum distance of 34,773 km on 14 December 1962. On 14 July 1965, the *US Mariner 4* spacecraft became the first spacecraft to successfully fly

by Mars at a minimum distance of 9,846 km. The first soft landing on Mars was performed by the *Mars 3* spacecraft, launched by the USSR in December 1971. Since then, many interplanetary spacecrafts have been launched by the USSR/Russia, USA, Europe (ESA) and Japan to perform flyby missions to all planets, flybys of comets, asteroids, and moons of planets, landings on Mars, Venus, Titan and asteroids, and an impact on a comet.

But even for this minimum-energy trajectory, the relatively low energy density and exhaust velocity of chemical propellants only allow the launch of relatively small payloads, in particular to the more distant planets.

In the early 1960s, a fundamental new concept of space travel was developed: the *swingby concept*, also known as the *gravity-assist concept*.

To reach a distant planet, the idea is to launch a S/C to an easy-to-reach nearby planet and to pass that planet on a precise trajectory such that planet's gravity field would change vehicle's orbital energy relative to the Sun.

The first spacecraft that has experienced a substantial gravity assist was *NASA's Pioneer 10*, which was launched on 3 March 1972, by an Atlas/Centaur rocket. In December 1973, it approached Jupiter.

Although it is possible to increase spacecraft's velocity relative to the Sun considerably, the application of the swingby technique will lead to long total flight times.

In a preliminary design for interplanetary missions, the most common method is the so-called "patched conics", which allows getting an approximate  $\Delta V$  and time of flight, at a low computational cost.

The method of patched conics is used to divide the mission up into three parts:

- the hyperbolic departure trajectory (generally geocentric) relative to home planet: escape. It is determined by the gravity field of the Earth;
- the cruise ellipse relative to the Sun: Hohmann transfer, the most energy-efficient way for a spacecraft to transfer from one planet's orbit to another (Figure 2.1)). It is determined by Sun's gravity field;
- the hyperbolic arrival trajectory relative to target plane: capture. Trajectory is considered as a planetocentric hyperbola that is solely determined by gravity field of that planet.

Consider Figure 2.1, which shows a Hohmann transfer from an inner planet 1 to an outer planet 2 (for example from Earth to Mars). The departure point D is at periastron (perihelion) of the transfer ellipse and the arrival point A is at apoastron (aphelion).

Each of them is studied as a two bodies' problem: it is assumed that if the satellite is outside the sphere of influence of a planet, the only effect to be taken into account is the gravitational attraction of the Sun. In the same way, if it is inside the sphere of influence of a planet, the attraction of the Sun will not be considered.

The first leg of the interplanetary mission is the most important for our study. For this reason, in the next section, it is the only one dealt examined in depth.

To simplify the beginning of our study of interplanetary trajectories, we will assume that all the planets' orbits are circular and coplanar.

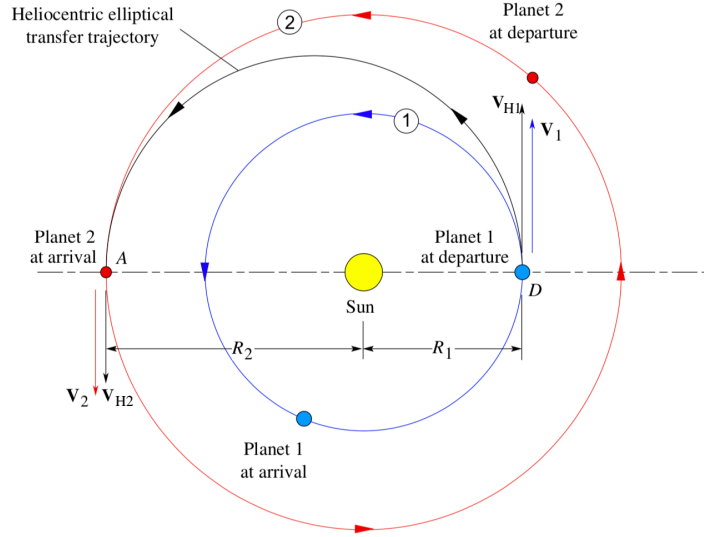


Figure 2.1: Hohmann transfer from inner planet 1 to outer planet 2 [4]

## 2.2 Escape

First of all, to obtain all the details of this leg, it is necessary to determine the heliocentric trajectory. This trajectory takes the S/C from the sphere of influence of planet 1 to that of planet 2, with an Hohmann transfer orbit.

After calculating the speed required by the elliptical transfer at the SOI of planet 1, it is possible to analyze the planetary departure.

As in Figure 2.1,  $V_1$  is the circular orbital speed of planet 1 relative to the Sun:

$$V_1 = \sqrt{\frac{\mu_S}{r_1}} \quad (2.1)$$

Since the elliptical transfer orbit has a semi-major axis of

$$a_H = \frac{r_1 + r_2}{2}, \quad (2.2)$$

the energy of this orbit is

$$\varepsilon = \frac{V^2}{2} - \frac{\mu}{r} = -\frac{\mu}{2a}. \quad (2.3)$$

It is easy to calculate the velocity of the space vehicle on the transfer ellipse at the departure point D:

$$V_{H1} = \sqrt{\frac{2\mu}{r_1} - \frac{2\mu}{r_1 + r_2}} \quad (2.4)$$

So, in our study, this is the heliocentric velocity of the S/C, at the boundary of Earth’s sphere of influence. It is parallel to the asymptote of the departure hyperbola as well as to the planet’s heliocentric velocity vector  $V_1$ .

In the geocentric reference, it can be obtained the required hyperbolic excess speed of the departure hyperbola manipulating the equation

$$V_{H1} = V_1 + V_\infty \quad (2.5)$$

It should be noted that only the magnitude are added up, not the vectors (only for Hohmann’s transfer).

It is important to underline that, the same considerations apply not only for Hohmann but for any trajectory, both ballistic and propelled (even with electric propulsion): from the point of view of the escape maneuver, all that matters are the magnitude and the direction of the required  $V_\infty$ .

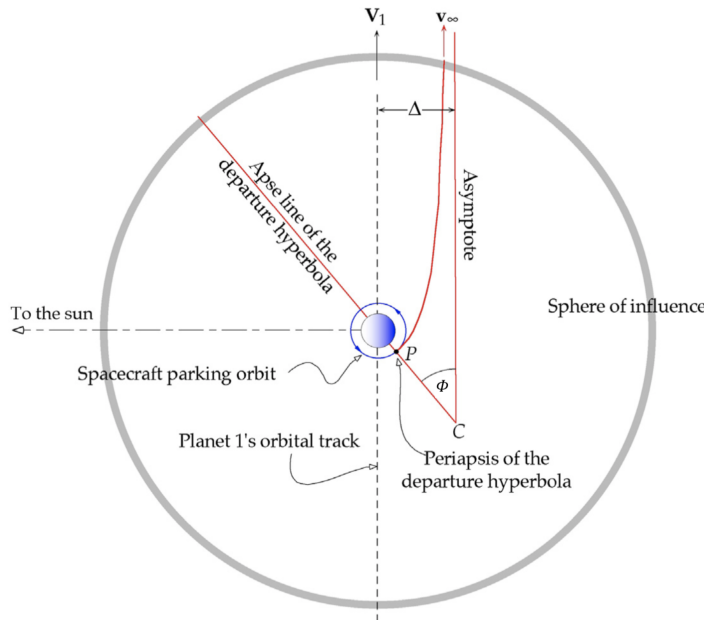


Figure 2.2: Departure of a spacecraft on a mission from an inner planet to an outer planet [4]

Coming back to the first leg, as usual, the spacecraft starts from a circular parking orbit, whose radius equals the perigee radius  $r_P$  of the departure hyperbola.

Known this value, and the hyperbolic excess velocity, from the energy it is easy to get the semi-major axis of the hyperbola and the  $\Delta V$  necessary to reach the exact trajectory.

$$\varepsilon = \frac{V_\infty^2}{2} = -\frac{\mu_E}{2a} \quad \text{so} \quad a = -\frac{\mu_E}{V_\infty^2} \quad (2.6)$$

$$\varepsilon = \frac{V_P^2}{2} - \frac{\mu_E}{r_P} = \frac{V_\infty^2}{2} \quad \text{so} \quad V_P = \sqrt{V_\infty^2 + \frac{2\mu_E}{r_P}} \quad (2.7)$$

with

$$\frac{\mu_E}{r_P} = V_{PO}^2$$

So, from the circular parking orbit it is required

$$\Delta V = V_P - V_{PO} \quad (2.8)$$

As in Figure 2.2,  $\Phi$  gives the orientation of the apse line of the hyperbola to planet's heliocentric velocity vector. To calculate it, it is necessary, first of all, to determine the eccentricity of the escape trajectory.

First, it is defined the semilatus rectum:

$$p = \frac{h^2}{\mu_E} = a(1 - e^2) = r_P(1 + e) \quad (2.9)$$

in which  $h$  is the angular momentum of the departure hyperbola (relative to the planet), and in our case is equal to

$$h = r_P V_{PO} \quad (2.10)$$

So, the eccentricity of the hyperbola it can be calculated as:

$$e = \frac{r_P V_{PO}^2}{\mu_E} - 1 \quad (2.11)$$

and therefore it is possible to calculate the  $\Phi$  angle as

$$\Phi = \arccos\left(\frac{1}{e}\right) \quad (2.12)$$

In the particular case, in which the S/C must be sent from an outer planet to an inner planet, then the spacecraft's heliocentric speed at departure must be less than that of the planet. For this reason, the spacecraft must emerge from the backside of the sphere of influence with its relative velocity vector directed opposite to  $V_1$ , the so-called *back door exit*, instead of *front door exit*.

## 2.3 Flyby

As mentioned before, the introduction of the *gravity-assist concept* was fundamental to reach the external solar system. So, in this section, it will be briefly exposed the concepts behind the flyby.

A planetary (or lunar) flyby occurs when a spacecraft, entered the SOI of that planet (or the Moon), does not impact or go into orbit around it. The S/C will continue in its hyperbolic trajectory through periapsis and exit the sphere of influence.

At the inbound crossing point, velocities assume values as defined in the equation 2.5. Moving from magnitudes to vectors

$$\bar{V}_{H1} = \bar{V}_1 + \bar{V}_{\infty 1} \quad (2.13)$$

Similarly, at the outbound crossing, we have

$$\bar{V}_{H2} = \bar{V}_1 + \bar{V}_{\infty 2} \quad (2.14)$$

The  $\Delta\bar{V}$  in the spacecraft's heliocentric velocity is

$$\Delta\bar{V} = \bar{V}_{H2} - \bar{V}_{H1} = (\bar{V}_2 + \bar{V}_{\infty 2}) - (\bar{V}_1 + \bar{V}_{\infty 1}) \quad (2.15)$$

that is

$$\Delta\bar{V} = \bar{V}_{\infty 2} - \bar{V}_{\infty 1} = \Delta\bar{V}_{\infty} \quad (2.16)$$

The hyperbolic excess velocity changes its direction but maintains the same magnitude, lie along the asymptotes of the hyperbola. As in Figure 2.3, are therefore inclined at the same angle  $\Phi$  to the apse line.

From this figure it can be seen that, in a trailing-side flyby, the component of  $\Delta\bar{V}$  in the direction of the planet's velocity is positive, whereas for leading-side flyby, it is negative. So, a trailing-side flyby results in a increase in the spacecraft's heliocentric speed (or geocentric, for a lunar flyby).

As in Figure 2.3,  $\hat{u}_v$  is the unit vector in the direction of the planet's heliocentric velocity  $\mathbf{V}$ , while  $\hat{u}_s$  is the unit vector pointing from the planet to the Sun.

$\alpha$  is the angle between planet's heliocentric velocity and S/C heliocentric velocity: it is the flight path angle  $\gamma$  of spacecraft's heliocentric trajectory when it encounters planet's SOI.

It should be noted that  $V_1^{(v)}$  is equal to  $V_{H1}$ , as previously defined.

Spacecraft velocity could be divided into  $V_{\perp}$  and  $V_r$ , whose modules respectively are equal to:

$$V_{\perp} = \frac{\mu_S}{h_1}(1 + e_1 \cos \theta_1) \quad (2.17)$$

$$V_r = \frac{\mu_S}{h_1}e_1 \sin \theta_1 \quad (2.18)$$

The magnitude of  $\bar{V}_{\infty 1}$  is computable as

$$V_{\infty} = \sqrt{\bar{V}_{\infty 1} \cdot \bar{V}_{\infty 1}} = \sqrt{\bar{V}_{H1}^2 + \bar{V}^2 - 2\bar{V}_{H1}V \cos \alpha_1} \quad (2.19)$$



It is important to note that

$$\theta_2 = \theta_1 + \pi - 2\Phi, \quad (2.25)$$

so the bigger is  $\Phi$ , the greater is the heliocentric velocity gain. When  $\theta_2$  decreases,  $\bar{V}_{\infty 2}$  and  $\bar{V}$  tend to become parallel with same sense: the best condition is when the two velocities are exactly parallel and so  $V_{H2}$  is the greatest possible.

At the opposite, it happens for leading-side flyby: the two velocities are still parallel, but with opposite sense. In this way, the planet holds the spacecraft back.

The use of gravity assist maneuvers it is also very helpful to change the orbital parameters of spacecraft's orbit. One of the most important is the inclination, whose variation can be estimated through the simplified model here described.

This maneuver allows the S/C velocity vector to rotate relative to the plane of the initial incoming orbit. The angle of rotation depends on both the gravitational capacity of the flyby body and on the location of the point at which the spacecraft enters the body's sphere of activity. Mainly, it depends on the mutual orientation of the two vectors  $\bar{V}_{\infty}$  and  $\bar{V}_1$  (or in our particular case, for a lunar flyby, between  $\bar{V}_{\infty}$  and  $\bar{V}_M$ ).

Figure 2.4 shows the sphere of possible locations of the end of vector  $\bar{V}_{\infty 2}$ , after the planetary flyby. This sphere is determined by the angle of rotation of the hyperbolic excess velocity  $\delta$ . Remember that  $V_1$ , as previously used, is the heliocentric velocity of the planet, while  $V_{H1}$  is the spacecraft heliocentric velocity.

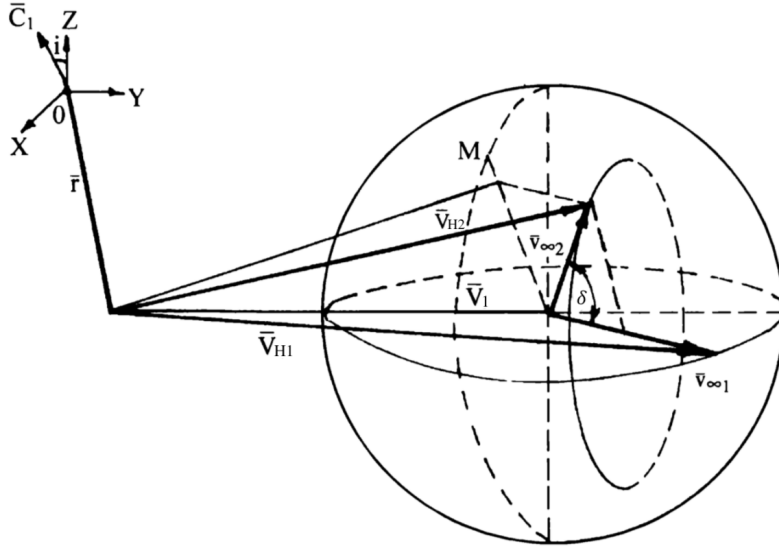


Figure 2.4: Changes in the inclination angle of the spacecraft orbit as result of gravity assist maneuver [8]

From this figure, it is possible to write the expression for the maximum change in the angle of inclination of the spacecraft orbital plane:

$$\sin \Delta i = \frac{\bar{V}_{\infty} \sin \delta}{V_1} \quad (2.26)$$

# Chapter 3

## Approximate analytical approach

### 3.1 Introduction

The solutions deriving from the approach that will be described in this chapter, are attempt solutions, necessary to then derive the numerical exact ones.

The analysis is based on a patched-conic approximation that neglects the dimension of Moon's sphere of influence. The trajectory is split into three geocentric legs:

1. the inner leg, from trajectory perigee (usually imposed by the launcher) to the Moon;
2. the intermediate leg, a Moon-to-Moon transfer;
3. the outer leg, from the Moon to the boundary of Earth's sphere of influence (set at 1 million km).

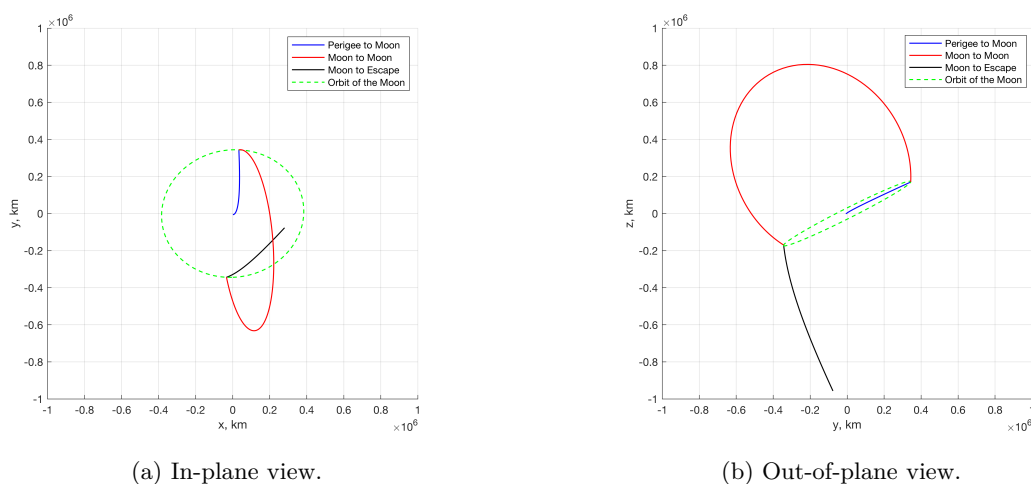


Figure 3.1: Lunar escape trajectory with backflip

LGA is modeled as an instantaneous relative velocity rotation at Moon’s intercept, which separates the geocentric legs.

This approach neglects all the external perturbations (as the influence of the Sun for example) and it considers only the influence of the gravitational force exercised by the Earth on the spacecraft (because the S/C remains inside the Earth’s sphere of influence).

An example of complete trajectory can be seen both in Figure 3.1 and 3.2, where the three legs are underlined by three different colors. The green dotted line represents Moon’s orbit. These trajectories correspond to the reference case, treated in the following.

All the characteristics of this particular trajectory with a double lunar flyby will be discussed, analyzed and compared in the next chapters.

However, you can immediately notice that the Moon–to–Moon leg is extremely inclined: that is because in this document a backflip transfer (section 3.2.2) will be treated.

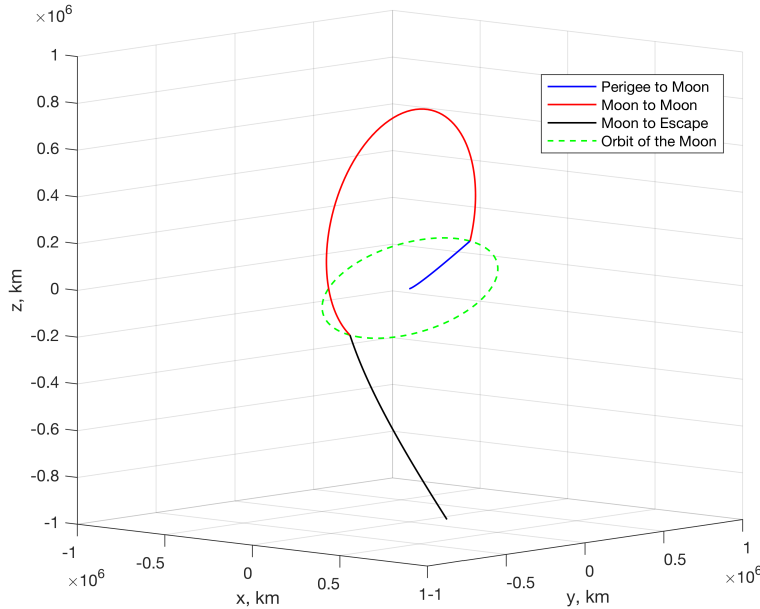


Figure 3.2: Approximate analytical solution, 3D view

## 3.2 Trajectory analysis

In this section, the trajectory will be analyzed backwards. In particular, the analysis is carried out with a reference frame based on Moon’s osculating orbit:  $x$ -axis towards the ascending node of Moon’s orbit with respect to Earth’s equator,  $z$ -axis along angular momentum,  $y$ -axis to complete a right-handed reference frame.

### 3.2.1 Moon to Escape

It is fundamental that Moon's orbit intercepts spacecraft escape hyperbola at one of the nodes. The escape velocity gives

$$a_3 = -\frac{1}{V_\infty^2 - 2/r_\infty} \quad (3.1)$$

Then, after calculating the unit vector along angular momentum

$$u_h = u_n \times V_\infty \quad (3.2)$$

with  $u_n$  unit vector pointing to the ascending node (it is important to notice that sign must change for negative  $V_{\infty,z}$ , as in all our cases visible at Table 5.1, Chapter 5), the inclination can be obtained from the angular momentum

$$i_3 = \arccos(u_{h,z}) \quad (3.3)$$

Another equation can be obtained from the position of the spacecraft at the second flyby, because the distance from the Earth must be the same for S/C and Moon. This kind of solution is approximated as it assumes first of all the modeling of the lunar orbit around the Earth as circular.

$$r_M = \frac{a_3(1 - e_3^2)}{1 + e_3 \cos(\nu_3)} \quad (3.4)$$

Moreover, it is important to note that there is a misalignment between the velocity directions at infinity and at the boundary of the sphere of influence, that is

$$\beta = \left(\frac{\pi}{2} - \nu_\infty + \gamma_\infty\right) - \Phi \quad (3.5)$$

because escape is actually reached at the boundary of the sphere of influence and not at infinity.

At escape, the true anomaly is obtained from

$$r_\infty = \frac{a_3(1 - e_3^2)}{1 + e_3 \cos \nu_\infty} \quad (3.6)$$

and the flight path angle is

$$\gamma_\infty = \arctan \frac{e_3 \sin \nu_\infty}{1 + e_3 \cos \nu_\infty} \quad (3.7)$$

$\beta$  is added to the rotation that must be provided by Moon's flyby.

### 3.2.2 Moon to Moon

Although three kinds of Moon to Moon transfer are possible, in this section only the one consider for our study will be presented and better described:

1. resonant transfers: the Moon is intercepted at the same place after a small integer number (e.g., 2:1) of revolutions;

2. planar transfers: the trajectory lies entirely on Moon's orbit plane.
3. backflip transfers: the case at hand.

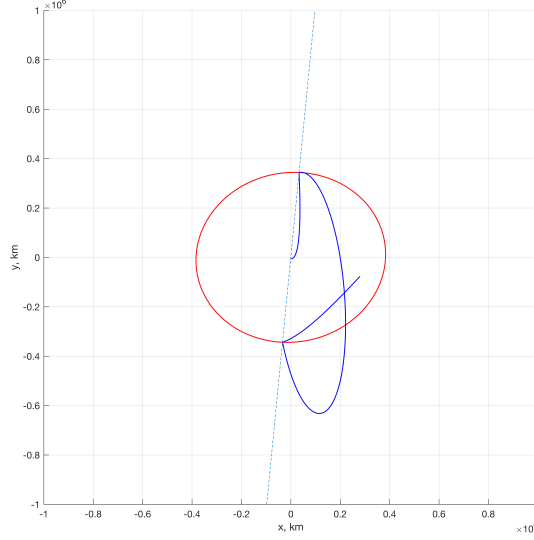


**Figure 3.3: Approximate analytical solution, XY plane**

In the last kind, the Moon is intercepted at points 180 degrees apart, that is, at the intersections of the spacecraft and Moon orbit planes. Moon's orbit is intercepted by spacecraft orbit at  $\pm 90$  degrees from its perigee.

As clearly visible in Figure 3.3, the two flybys occur, in a geocentric reference, in positions symmetrically opposite to the Earth.

So,

$$p_2 = r_M \quad \text{and} \quad \nu_{fb} = \pm\pi/2.$$

Since this document aims to describe only short maneuvers (to avoid large distances from the Earth), only intercept of the Moon after 1.5 revolution is considered, with the spacecraft performs either 0.5 or 1.5 revolutions.

The inclination could be obtained from

$$\frac{1}{a_2} + 2\sqrt{\frac{a_2(1-e_2^2)}{r_M^3}} \cos i_2 = \frac{3}{r_M} - V_\infty^2 \quad (3.8)$$

which is solved for  $e_2$  given the inclination. The nonlinear system is solved numerically, by introducing the ratio of periapsis radius to Moon's orbit radius

$$\rho = \frac{r_p}{r_M}$$

And so,

$$e_2 = \frac{1 - \rho}{\rho - \cos \nu_{fb}} \quad (3.9)$$

$$a_2 = \frac{\rho}{1 - e_2} r_M \quad (3.10)$$

### 3.2.3 Perigee to Moon

As before, intercept is on the reference plane and must occur at a node of the spacecraft orbit. Since the magnitude of the relative velocity before and after the flyby must be the same, the following equation can be derived

$$(V_\infty^2 - 3/r_M) + (1 - e_1)/r_P = -2\sqrt{r_P/r_M^3} \cos i_1 \sqrt{1 + e_1} \quad (3.11)$$

in which the larger solution (plus sign) is for prograde orbits ( $i_1 \leq \pi/2$ ), the lower one for retrograde orbits ( $i_1 \geq \pi/2$ ).

From the vectors  $\mathbf{V}_{\infty+}$  and  $\mathbf{V}_{\infty-}$ , it is possible to estimate the angle of rotation of the velocity at both flybys

$$\delta = 2 \arcsin \frac{\mu_M/r_{ps}}{V_\infty^2 + \mu_M/r_{ps}} \quad (3.12)$$

with  $r_{ps}$  the flyby periselenium, which can be determined by inverting the equation. As already mentioned, for the second flyby, the rotation is  $\delta + \beta$ .

The values of position and velocity at perigee ( $V_P$ ) are then rotated to the J2000 geocentric frame to determine the corresponding latitude, longitude and azimuth. Azimuth and  $\Delta V_P = V_P - V_C$  can be used to evaluate the mass that the launcher can insert into the escape trajectory.

In particular, all the calculations are made for the *Delta IV Heavy* rocket. The starting mass on the initial 200-km parking orbit is the sum of useful mass ( $m_u$ ) and upper stage dry mass  $m_d$  (3550 kg). The useful mass given by *NASA's Launch Vehicle Performance Website* is here approximated with the quadratic equation

$$m_u = 26280 - 0.6642(A - 90)^2 \quad (3.13)$$

where  $m_u$  is in kg and the azimuth  $A$  in degrees. The useful escape mass is evaluated with the rocket equation

$$m_\infty = (m_u + m_d)e^{-\Delta V/c} - m_d - m_{PAF} \quad (3.14)$$

where the stage dry mass and the payload attach fitting mass (800 kg) are subtracted from the final mass. And also,

$$\Delta V = 1.046(V_p - V_{PO}) \quad (3.15)$$

as  $V_P$  is the perigee velocity at the start of the trajectory to the Moon, and  $V_{PO}$  is the circular velocity on the parking orbit. An addition of a 4.6% margin has been added to attain a reference value of 9995 kg for the escape mass when  $C3 = -1.5 \text{ km}^2/\text{s}^2$ .

### 3.3 Calculations

Software gives us the following information, in the geocentric reference:

1. position and velocity of the S/C at the perigee;
2. position and velocity of the S/C before the first flyby;
3. position and velocity of the S/C after the first flyby and velocity of the Moon;
4. position and velocity of the S/C before the second flyby and velocity of the Moon;
5. position and velocity of the S/C after the second flyby;
6. position and velocity of the S/C at the boundary of the sphere of influence.

In particular, Moon's velocity is unchanged before and after the same flyby, and for this reason is reported only once.

Furthermore, at the two flybys, position coincides both for spacecraft and Moon in the model used to do the calculations. However the spacecraft will pass at a distance  $r_P$ , the periselenium, calculated with respect to the center of mass of the Moon.

From this data, it was possible to calculate the classical orbital parameters for the three legs in which trajectory were split, for example as illustrated in section 4.4 of the *Curtis, Howard D.* [4], knowing the components of  $r$  and  $V$ .

Then, were calculated the  $V_\infty$

$$\begin{cases} \overline{V}_{\infty 1-} = \overline{V}_{1-} - \overline{V}_{M1} \\ \overline{V}_{\infty 1+} = \overline{V}_{1+} - \overline{V}_{M1} \end{cases} \quad (3.16)$$

Where  $V_{\infty-}$  indicates the velocity before the first flyby,  $V_{\infty+}$  after it, while,  $V_{1-}$  and  $V_{1+}$  are the velocities of the spacecraft before and after the first flyby.  $V_M$  is the velocity of the Moon.

These two equations and all those that follow are the same for the second flyby too.

From these vectors, it was possible to determine the angle of rotation given by the flyby, simply applying the scalar product

$$\delta_1 = \arccos \frac{\overline{V}_{\infty 1-} \cdot \overline{V}_{\infty 1+}}{|\overline{V}_{\infty 1-}| |\overline{V}_{\infty 1+}|} \quad (3.17)$$

As said before, the S/C at both flybys passes at a certain distance from the Moon, computable from the patched conics model, by inverting the equation 3.12

$$r_{P1} = \frac{\mu_M(1 - \sin(\delta_1/2))}{\sin(\delta_1/2)V_{\infty 1}^2} \quad (3.18)$$

Known the magnitude, the unit vector ( $\hat{d}r$ ) is taken from

$$\hat{d}r_1 = \begin{bmatrix} (V_{\infty-1,x} - V_{\infty+1,x}) / (|\overline{V}_{\infty 1-}| - |\overline{V}_{\infty 1+}|) \\ (V_{\infty-1,y} - V_{\infty+1,y}) / (|\overline{V}_{\infty 1-}| - |\overline{V}_{\infty 1+}|) \\ (V_{\infty-1,z} - V_{\infty+1,z}) / (|\overline{V}_{\infty 1-}| - |\overline{V}_{\infty 1+}|) \end{bmatrix} \quad (3.19)$$

So, to sum up, the position with respect to the Moon is

$$\bar{d}r_1 = r_{P1} \cdot \hat{d}r_1 \quad (3.20)$$

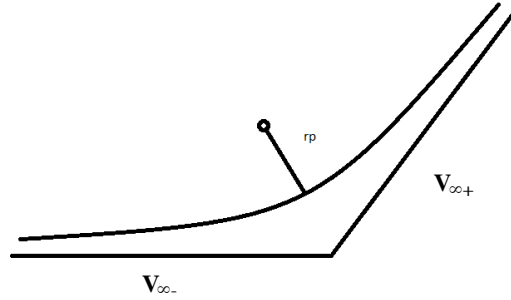


**Figure 3.4: Position at the flyby, with respect to the Moon**

While, in the geocentric reference, the position of the spacecraft at both flybys is obtained by adding to the position of the Moon (given by the software), the vector calculated by equation 3.20

At last,  $\vartheta$  and  $\phi$  were calculated in the geocentric reference by the vectors' components seen above through trigonometry.



## Chapter 4

# Exact numerical solution

### 4.1 Solution description

In order to obtain spacecraft trajectory, in this document, an indirect method has been used. Indirect methods, are widely used to solve ODE boundary problems (*BVP*). In particular BVP has been solved by means of shooting procedures.

The *shooting methods*, solve numerically the BVP problem by reducing it to the initial value problem (IVP). We 'shoot' out trajectories in different directions until we find a trajectory that has the desired boundary value. This method allows you to estimate the initial conditions.

The use of this method, provides many advantages, among which: allows you to get a numerical exact optimization, the computational cost of indirect methods is typically lower compared to direct methods and provides useful theoretical information on the problem to be solved. Obviously, are also some downsides: first, it is required to derive analytic expressions for the necessary conditions; second, the convergence region for a shooting algorithm may be quite small.

To achieve convergence to the solution, it is extremely important to begin with an appropriate *tentative solution*, as it can be seen in the next chapters. In particular, for this document, the *tentative solution* is obtained via the solution of a similar but easier problem.

The system is described by a set of state variables  $\bar{x}$ ; differential equations rule the evolution from the initial to the final state

$$\frac{d\bar{x}}{dt} = f(\bar{x}, \bar{u}, t) \quad (4.1)$$

functions of  $\bar{x}$ , of the control variables  $\bar{u}$ , and the independent variable  $t$  (usually, the time).

The problem has the same number of parameters and of imposed conditions: considering the trajectory as a whole, the parameters are

$$(t_f - t_0), \vartheta_0, \varphi_0, v_0, w_0$$

while the imposed conditions are:

$$u_f, v_f, w_f, r_f, i_0(\text{inclination}).$$

At first, the trajectory was split only in two phases: first one from perigee (circular parking orbit) to the first flyby, second one from this point to the escape. So, the whole problem has a single solution, because the number of free parameters is equal to the number of conditions.

Due to numerical convergence problem, another two inner phases were added. Therefore, on the whole, trajectory was divided into four phases:

1. From perigee to first flyby;
2. from first flyby to apogee;
3. from apogee to second flyby;
4. from second flyby to escape.

Among which, there are three internal boundaries, where the state variables are discontinuous or constraints are imposed:

- first periselenium;
- apogee;
- second periselenium.

Considering internal points, for each one we add a parameter (time) and a condition (relative velocity perpendicular to vector (S/C – Moon) for the periselenium,  $u = 0$  at the apogee).

By the division of the trajectory into 4 legs, the *shooting method* became the *multiple shooting method*. In the multiple shooting, variables are added after the apogee as parameters and continuity equations as conditions.

The method solves an initial value problem in each of the smaller intervals, and imposes additional matching conditions to form a solution on the whole interval. The division into smaller intervals guarantees improvement on numerical stability over single shooting methods. So, all in all, are solved four BVP transformed into IVP.

Furthermore, nonlinear constraints at both internal and external boundaries are imposed. In general, these boundary conditions are grouped into a vector  $\bar{\Psi}$

$$\Psi(\bar{x}_{(j-1)_+}, \bar{x}_{j-}, t_{(j-1)_+}, t_{j-}) = 0 \quad j = 1, \dots, n \quad (4.2)$$

where the  $j$ th arc starts at  $t_{(j-1)_+}$  and ends at  $t_{j-}$  (– and + denote values just before and after point  $j$ ).

The initial values of some of the variables are usually unknown, and the search for the solution results is determined, through an iterative process. Known the initial values at the  $r$ -th iteration, into  $\bar{p}^r$ , obtained through the previous iteration. Then, the equations must be integrated along the whole trajectory, taking into account any discontinuities in

the internal boundaries. Obviously,  $\bar{p}^1$  is derived from the tentative solution. At the end of the integration the errors on the boundary conditions are calculated.

Then, a  $\Delta\bar{p}$  that varies the error on the boundary conditions, is applied. In particular, the unknowns are in turn varied by a small amount to evaluate the derivatives of the errors with respect to the unknowns, according to a forward-finite-difference scheme. Newton's method is used to bring the errors to zero.

Taking into account only the terms of the first order, you get:

$$\Delta\bar{\Psi} = \left[ \frac{\partial\bar{\Psi}}{\partial\bar{p}} \right] \Delta\bar{p} \quad (4.3)$$

So, in order to undo the error on the boundary conditions (i.e.  $\Delta\bar{\Psi} = -\bar{\Psi}^r$ ), at each iteration the initial values are corrected as

$$\Delta\bar{p} = \bar{p}^{r+1} - \bar{p}^r = \left[ \frac{\partial\bar{\Psi}}{\partial\bar{p}} \right]^{-1} \bar{\Psi}^r \quad (4.4)$$

until the boundary conditions are verified with the desired accuracy. Actually, in order to not get too far from the solution, only a fraction of the correction is made:

$$\bar{p}^{r+1} = \bar{p}^r + K_1\Delta\bar{p} \quad (4.5)$$

where  $K_1 = 0.1 - 1$ .

A significant example, is here reported, derived from a tentative solution of one of the cases studied in the next chapters (this is not the first tentative solution, it is the last one before convergence).

From this example it is possible to evaluate which are the unknowns. Between them, there are four times (the final one and the other three due to the internal points), six variables that refer to the apogee in terms of positions and velocity components and five that refer to the initial condition (as shown schematically in the Figure 4.1). In particular, all the values in figure, for the first iteration, are obtained from the tentative solution as already mentioned in Chapter 3.

$r_0$  is not an unknown (as can be noted previously) because the circular parking orbit is known. Moreover, the initial mass is equal to 26280 kg.

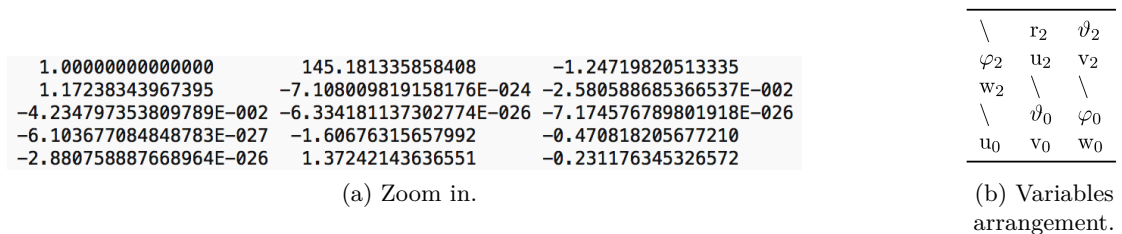


Figure 4.1: Software solution output

To sum up, in total there are 15 unknowns and there are the same number of conditions. In particular these are:

- seven conditions at the escape (escape date, escape position components  $x y z$  and escape velocity components  $u v w$ );
- radial velocity at the apogee was stated equal to zero ( $u = 0$ );
- dot product between relative velocity and the relative distance at the second periselenium equal to zero (perpendicular vectors);
- six continuity equations between phase 2 and 3 for  $r, \vartheta, \varphi, u v$  and  $w$ .

Moreover, as previously mentioned, to have a continuous solution, at the internal boundaries must be imposed continuity in terms of position and velocity.

Among all the outputs, extremely important will be the comparison between Moon's position and spacecraft's position at both flybys. This aspect will be analyzed in the following chapter, and one will understand the importance of relative positions.

## 4.2 Equations

The spacecraft is modeled as a point with variable mass. Position  $\bar{r}$ , velocity  $\bar{v}$ , and mass  $m$  of the spacecraft are the problem state variables, described by differential equations

$$\begin{cases} \frac{d\bar{r}}{dt} = \bar{v} \\ \frac{d\bar{v}}{dt} = -\frac{\mu\bar{r}}{r^3} + \frac{\bar{T}}{m} + \bar{a}_P \\ \frac{dm}{dt} = -\frac{T}{c} \end{cases} \quad (4.6)$$

The thrust vector  $\bar{T}$  in this document is assumed to be zero.  $\bar{a}_p$  is the perturbing acceleration, given by

$$\bar{a}_P = \bar{a}_J + \bar{a}_{lsg} + \bar{a}_{srp} \quad (4.7)$$

where:  $\bar{a}_J$  is the perturbation due to the Earth asphericity,  $\bar{a}_{lsg}$  the luni-solar gravity and  $\bar{a}_{srp}$  is the solar radiation pressure.

It is adopted the *EME2000* reference frame (Earth Mean Equator and Equinox of Epoch J2000):  $\hat{I}$ ,  $\hat{J}$ , and  $\hat{K}$  are unit vectors along the axes of *EME2000*.

The position is expressed by spherical coordinates radius  $r$ , right ascension  $\vartheta$  and declination  $\varphi$

$$\bar{r} = r \cos \vartheta \cos \varphi \hat{I} + r \sin \vartheta \cos \varphi \hat{J} + r \sin \varphi \hat{K} \quad (4.8)$$

It is also defined a topocentric reference frame, whose unit vectors are  $\hat{i}$  (radial),  $\hat{j}$  (eastward), and  $\hat{k}$  (northward).

It can be written

$$\begin{Bmatrix} \hat{i} \\ \hat{j} \\ \hat{k} \end{Bmatrix} = \begin{bmatrix} \cos \vartheta \cos \varphi & \sin \vartheta \cos \varphi & \sin \varphi \\ -\sin \vartheta & \cos \vartheta & 0 \\ -\cos \vartheta \sin \varphi & -\sin \vartheta \sin \varphi & \cos \varphi \end{bmatrix} \cdot \begin{Bmatrix} \hat{I} \\ \hat{J} \\ \hat{K} \end{Bmatrix} \quad (4.9)$$

So, in this frame, the position is easily expressed as  $\bar{r} = r \hat{i}$ , while the velocity as

$$\bar{v} = \dot{\bar{r}} = u\hat{i} + v\hat{j} + w\hat{k} \quad (4.10)$$

with  $u$ ,  $v$ , and  $w$  being radial, eastward, and northward components, respectively. The scalar state equations can be expressed as

$$\begin{cases} \frac{dr}{dt} = u \\ \frac{d\vartheta}{dt} = \frac{v}{r(\cos \varphi)} \\ \frac{d\phi}{dt} = \frac{w}{r} \\ \frac{du}{dt} = -\frac{\mu}{r^2} + \frac{(v^2+w^2)}{r} + \frac{T_u}{m} + (a_P)_u \\ \frac{dv}{dt} = \frac{(-uv+vw \tan \varphi)}{r} + \frac{T_v}{m} + (a_P)_v \\ \frac{dw}{dt} = \frac{(-uv+v^2 \tan \varphi)}{r} + \frac{T_w}{m} + (a_P)_w \\ \frac{dm}{dt} = -\frac{T}{c} \end{cases} \quad (4.11)$$

It must be remembered that the thrust  $T$  is assumed to be zero, along the whole trajectory.

### 4.3 Perturbations

In this model, that implements perturbations, the following will be considered:

- perturbation due to the Earth asphericity;
- perturbation due to the gravitational attraction of the Sun;
- perturbation due to the gravitational attraction of the Moon;
- pressure of solar radiation.

In addition, it will be considered the eccentricity of Moon's orbit.

### 4.3.1 Earth asphericity

To take into account the perturbation due to the Earth asphericity, for this thesis it is used the Earth potential description, based on the *Earth Gravitational Model EGM200*. It provides normalized spherical harmonic coefficients for the Earth gravitational potential. The potential corresponding to the Earth asphericity is expressed as

$$\Phi = -\frac{\mu_E}{r} \sum_{n=2}^N \left(\frac{r_E}{r}\right)^n \sum_{m=0}^n (C_{nm} \cos m\lambda + S_{nm} \sin m\lambda) P_{nm}(\sin \varphi) \quad (4.12)$$

where  $r_E$  is the semi-major axis of the Earth ellipsoid.  $N$  is set to 8: it is considered an  $8 \times 8$  model of the Earth gravitational potential.  $P_{nm}(\sin \varphi)$  is the associated Legendre functions while  $C_{nm}$  and  $S_{nm}$  are the spherical harmonic coefficients. The declination  $\varphi$  corresponds to the terrestrial latitude, while terrestrial longitude  $\lambda$  is obtained as  $\lambda = \vartheta - \vartheta_{\text{Gref}} - \omega_E (t - t_{\text{ref}})$  where  $\vartheta_{\text{Gref}}$  is the Greenwich right ascension at the reference time  $t_{\text{ref}}$ .

From the calculation of the gradient of  $-\Phi$ , it is obtain the perturbing acceleration due to the Earth asphericity. Its components in the topocentric frame are

$$\begin{cases} (a_J)_u = -\frac{\partial \Phi}{\partial r} \\ (a_J)_v = -\frac{(\partial \Phi / \partial \vartheta)}{(r \cos \varphi)} \\ (a_J)_w = -\frac{(\partial \Phi / \partial \varphi)}{r} \end{cases} \quad (4.13)$$

Derivatives with respect to  $\varphi$  require the derivatives of the associated Legendre functions, which are obtained recursively.

### 4.3.2 LuniSolar perturbation

The lunisolar perturbation is the sum of the gravitational perturbations due to Moon and Sun. Positions of Sun and Moon are evaluated by DE405 JPL ephemeris [16]. It provides the body position in rectangular coordinates  $x_b$ ,  $y_b$  and  $z_b$  with respect to the Earth. Subscript  $b$  could be  $s$  for Sun or  $l$  for Moon.

The perturbing acceleration on the spacecraft

$$\bar{a}_{bg} = -\left(\frac{\mu_b}{R^3}\right) \bar{R} - \left(\frac{\mu_b}{r_b^3}\right) \bar{r}_b \quad (4.14)$$

is caused by a body with gravitational parameter  $\mu_b$ , whose position vector relative to the Earth is  $\bar{r}_b = x_b \hat{I} + y_b \hat{J} + z_b \hat{K}$ . Where  $\bar{R} = \bar{r} - \bar{r}_b$ , is the spacecraft relative position vector with respect to the perturbing body and  $-\bar{r}_b$  is the Earth relative position, as can be seen in Figure 4.2.

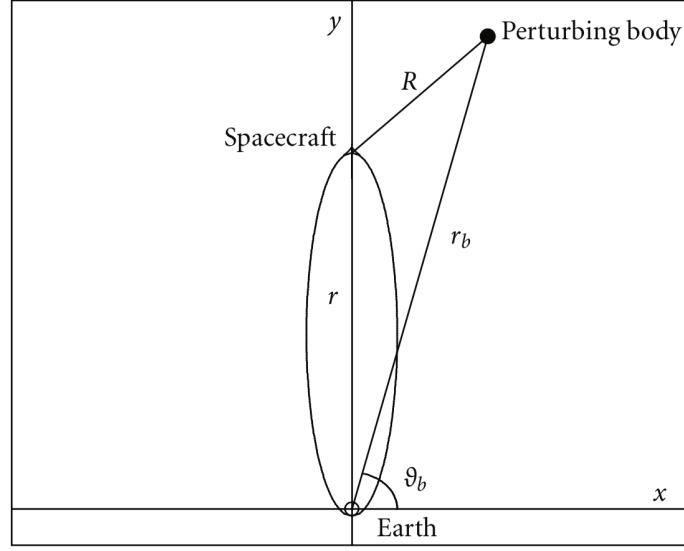


Figure 4.2: Schematic geometry of gravitational perturbations [5].

The perturbing acceleration is not composed only by the gravitational acceleration that the perturbing body causes on spacecraft, but also on the Earth. In the topocentric frame (based on the spacecraft position), it can be written as

$$\begin{cases} (\bar{a}_{bg})_u = \left(\frac{\mu_b}{R^3}\right) [(r_b)_u - r] - \left(\frac{\mu_b}{r_b^3}\right) (r_b)_u \\ (\bar{a}_{bg})_v = \left(\frac{\mu_b}{R^3}\right) (r_b)_v - \left(\frac{\mu_b}{r_b^3}\right) (r_b)_v \\ (\bar{a}_{bg})_w = \left(\frac{\mu_b}{R^3}\right) (r_b)_w - \left(\frac{\mu_b}{r_b^3}\right) (r_b)_w \end{cases} \quad (4.15)$$

with

$$R = \sqrt{[r - (r_b)_u]^2 + (r_b)_v^2 + (r_b)_w^2}$$

In this frame, the position components of the perturbing body  $b$  is given by

$$\begin{cases} (r_b)_u = x_b \cos \vartheta \cos \varphi + y_b \sin \vartheta \cos \varphi + z_b \sin \varphi \\ (r_b)_v = -x_b \sin \varphi + y_b \cos \vartheta \\ (r_b)_w = -x_b \cos \vartheta \sin \varphi - y_b \sin \vartheta \sin \varphi + z_b \cos \varphi \end{cases} \quad (4.16)$$

### 4.3.3 Solar radiation pressure

For this perturbation, it must be taken into consideration the photon pressure: at a distance  $R$  from the Sun, it can be evaluated as

$$p = L_s / 4\pi R^2 c_{light}$$

where  $L_s$  is the total power radiated by the Sun and  $c_{light}$  is the speed of light. At a distance  $R = 1$  AU,  $p = 4.55682 \cdot 10^{-6}$  N/m<sup>2</sup>. The acceleration on a spherical body is

$$\bar{a}_{srp} = (1 + \eta)p^* \left(\frac{R^*}{R}\right)^2 \left(\frac{S}{m}\right) \frac{\bar{R}}{R} = \frac{\Gamma \bar{R}}{mR^3} \quad (4.17)$$

with  $S$  the cross-section,  $m$  the mass of the spacecraft and  $\eta$  the reflectivity. Projected onto the topocentric frame

$$\begin{cases} (a_{srp})_u = \left[\frac{\Gamma}{mR^3}\right] [(r_s)_u - r] \\ (a_{srp})_v = \left[\frac{\Gamma}{mR^3}\right] [(r_s)_v] \\ (a_{srp})_w = \left[\frac{\Gamma}{mR^3}\right] [(r_s)_w] \end{cases} \quad (4.18)$$

Since the solar radiation pressure acts along the Sun-spacecraft direction, this acceleration is parallel but with opposite directions to the solar gravity acceleration.

In the equation 4.17 it can be noted that, unlike equation 4.14, the perturbing acceleration depends on the instantaneous mass.

## Chapter 5

# Approximate analytical approach results

### 5.1 Features

The results reported refer to 5 different escape conditions, at the boundary of the Earth's sphere of influence. Among these, the first 3 (cases 0, 2 and 4) have the same escape date (21/06/2022) but increasing  $V_\infty$ . However, with regard to the cases 4, 5 and 6 have the same  $V_\infty$  but antecedent escape date.

It is important to notice that, in the table below (Table 5.1),  $r$ ,  $\vartheta$  and  $\varphi$  are those of the Earth in its heliocentric motion:

- distances are expressed in AU;
- velocities are the relative ones of the S/C with respect to the Earth;
- velocities are dimensioned with the velocity of the Earth around the Sun (the reference is heliocentric-ecliptic):

$$V_E = \sqrt{\frac{\mu_S}{r_{S-E}}} \approx 29,78 km/s \quad (5.1)$$

First of all, the 5 different cases are defined.

Table 5.1: Escape conditions

	Case 0	Case 2	Case 4	Case 5	Case 6
$\mathbf{r}$	1,016193	1,016193	1,016193	1,016111	1,016023
$\vartheta$	4,702943	4,70294	4,702943	4,683577	4,664207
$\varphi$	4,843999E-5	4,84399E-5	4,84399E-5	4,84882E-5	4,85183E-5
$\mathbf{u}$	-3,6668E-3	-3,9547E-3	-4,2507E-3	-4,53042E-3	-4,8141E-3
$\mathbf{v}$	1,66059E-2	1,69436E-2	1,72617E-2	1,70068E-2	1,67514E-2
$\mathbf{w}$	-4,0197E-2	-4,1853E-2	-4,3513E-2	-4,3585E-2	-4,3653E-2
<b>Escape date</b>	21/ 6/2022	21/ 6/2022	21/ 6/2022	19/ 6/2022	18/ 6/2022
$\mathbf{V}_\infty$	1,3	1,35	1,4	1,4	1,4

As previously said, this conditions refer to an Asteroid Redirect Mission. In particular, the asteroid to be reached is *2008EV5*. This asteroid, of the Aten group (a group of asteroids, whose orbit brings them into proximity with Earth, with a semi-major axis of less than 1 AU and with an high eccentricity), was first observed on 4 March 2008. EV5 rotates retrograde and its overall shape is a  $400 \pm 50$  m oblate spheroid, so is defined as a sub-kilometer asteroid. It is a near-Earth object and potentially hazardous. On 23 December 2008, 2008EV5 made a close approach to Earth at a distance of 3.2 million km (0,022 AU), its closest until 2169. It has a semi-major axis of 0,958242 AU, an eccentricity of 0,083401 and an inclination of 7,437 degrees.

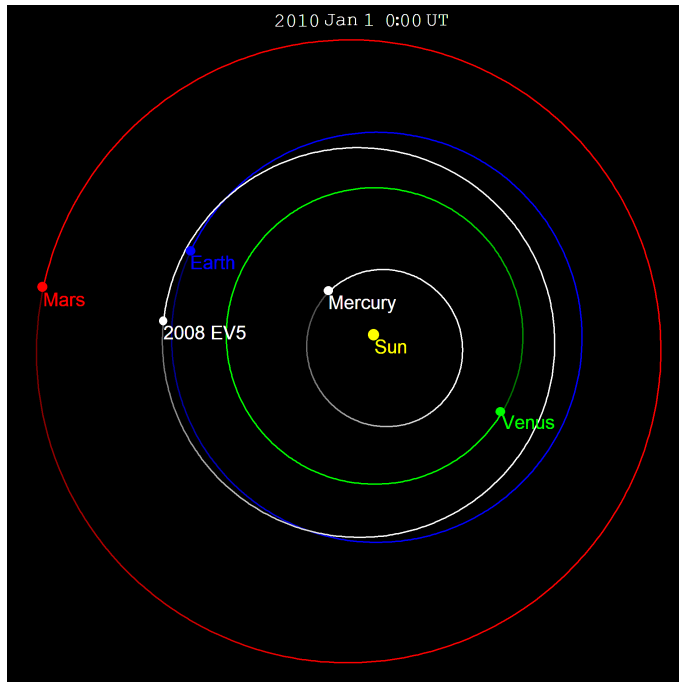


Figure 5.1: Asteroid 2008 EV5's orbit (white) compared with the nearest planets, in the heliocentric reference system [14].

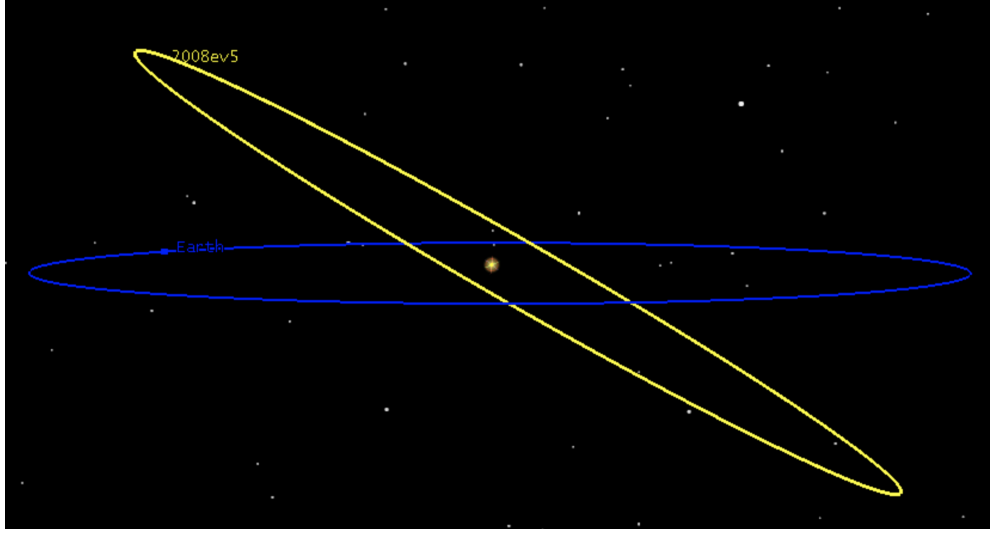


Figure 5.2: 3D visual of the asteroid and Earth orbit in the heliocentric reference system [14].

As you can see, in all 5 cases presented, the component with the highest magnitude is  $w$ . The latter, appears to be an order of magnitude greater than  $u$  and about double or triple of  $v$ , so the off-plane component is predominant, with respect to those on the plane.

Now that all the cases have been defined, solutions can be evaluated. First of all, it is presented the case 0, which will then be treated as the reference case. Then, are reported and analyzed the solutions separately between those with the same escape date and those with the same  $V_\infty$ .

## 5.2 Case 0 (comparison between exact and approximated solution)

In this section we will present the solution of the reference case with a comparison between the approximate and the exact numerical solution.

The following tables (also of the following chapter), express the positions of spacecraft and moon in spherical coordinates (radius  $r$ , longitude  $\vartheta$  and latitude  $\varphi$ ), at distinct points of the trajectory like the two flybys, the departure (from a LEO orbit) and the escape.

The magnitude of the radii is adimensionalized with respect to the terrestrial radius (6378,14 km), while the velocities with respect to the corresponding circular speed:

$$\sqrt{\frac{\mu_E}{r_E}} \quad (5.2)$$

Instead, as the name implies, the radius of periselenium is measured with respect to the centre of the Moon and again, the adimensionalized value is calculated as the other radii.

The velocity has a radial component  $u$  (i.e. towards the Zenit), one in the east direction  $v$  and a northward  $w$ . The classical orbital parameters were used (semi-major axis, eccentricity, inclination, longitude of the ascending node, argument of perapsis and true anomaly).

**Table 5.2: Comparison of S/C-Moon positions at the two flybys between exact and approximate solution**

	<b>Parameter</b>		<b>Exact</b>	<b>Approximated</b>
<b>FB1</b>	r	S/C	64,30886	60,56857
		Moon	64,02390	60,33634
	$\vartheta$	S/C	1,26703	1,34469
		Moon	1,26452	1,34238
	$\varphi$	S/C	0,42132	0,43526
		Moon	0,42692	0,44035
<b>FB2</b>	r	S/C	56,26755	60,04843
		Moon	56,59549	60,33634
	$\vartheta$	S/C	4,41875	4,48059
		Moon	4,42317	4,48397
	$\varphi$	S/C	-0,42654	-0,43773
		Moon	-0,43008	-0,44035

The distances at which the flyby occur are extremely different given that only in the exact numerical solution it is considered Moon's eccentricity

**Table 5.3: Comparison of relative positions at the two flybys between exact and approximate solution**

	<b>Parameter</b>	<b>Exact</b>	<b>Approximated</b>
<b>FB1</b>	$\vartheta_{SC}-\vartheta_M$	0,00251234	0,002312319
	$\varphi_{SC}-\varphi_M$	-0,00560428	-0,005092084
	$r_{\text{periselenium}}$	0,48176806	0,4059
	$r_{\text{periselenium}}$ [km]	3072,78235	2588,885524
<b>FB2</b>	$\vartheta_{SC}-\vartheta_M$	-0,004428128	-0,003376191
	$\varphi_{SC}-\varphi_M$	0,00353543	0,002615465
	$r_{\text{periselenium}}$	0,446113524	0,3762
	$r_{\text{periselenium}}$ [km]	2845,37283	2399,454876

You can appreciate that, even changing the model, relative positions maintain the same sign (in terms of  $\Delta\vartheta$  and  $\Delta\varphi$ , where a positive value indicates that the spacecraft is forward or higher than the Moon). The biggest difference is found in the distances between S/C and Moon at both flybys (the so-called radius of periselenium), with the largest values calculated from the exact numerical solution. Remember that Moon's radius is equal to 1737 km. During the first flyby the spacecraft is located at an altitude of only 1335 km from the lunar surface, while, at the second flyby, the altitude is lower

and is about 1108 km.

Table 5.4: Comparison of S/C positions between exact and approximate solution

	Parameter	Exact	Approximated
<b>Perigee</b>	r	1,03020	1,03020
	$\vartheta$	-1,60680	-1,54073
	$\varphi$	-0,47	-0,36676
<b>FB1</b>	r	64,30886	60,56857
	$\vartheta$	1,26703	1,34469
	$\varphi$	0,42132	0,43526
<b>FB2</b>	r	56,26755	60,04843
	$\vartheta$	4,418746267	4,48059
	$\varphi$	-0.4265	-0,43773
<b>Escape</b>	r	156.7856	156,78561
	$\vartheta$	0,0314	-0,41
	$\varphi$	-1,3333	-1,32022

At both flybys, the values of  $\vartheta$  calculated through the approximated model are greater than those calculated with the exact model. As visible in the figures below (Figure 5.3 and 5.4), where the blue line refers to the Moon’s orbit in the case of the most complex solution while, the red one it is relative to the simplest one.

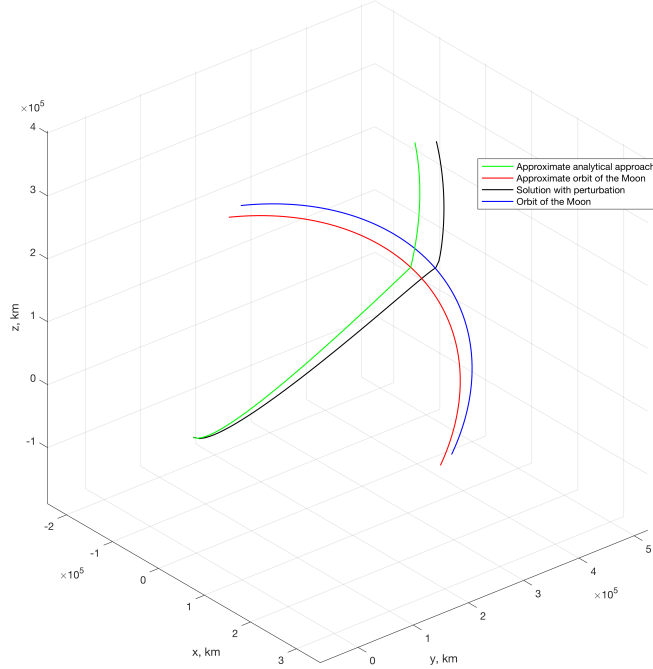


Figure 5.3: Zoom on FB1, comparison between exact and approximate solution

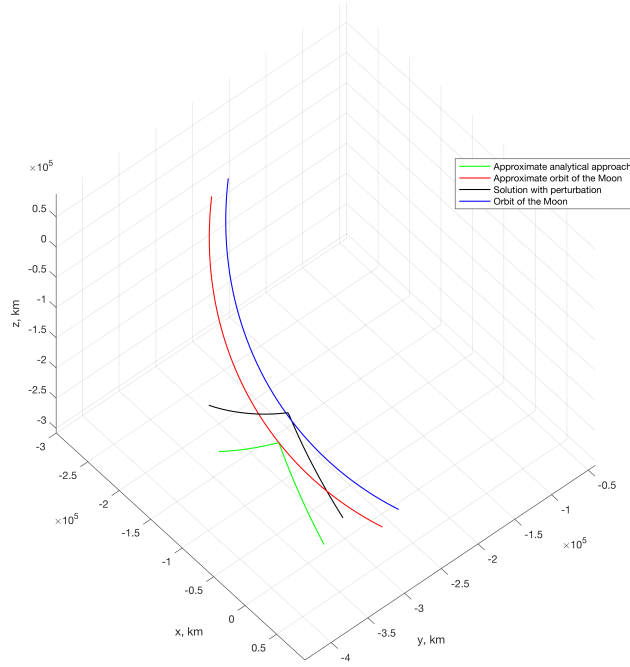


Figure 5.4: Zoom on FB2, comparison between exact and approximate solution

Furthermore, it can be noted that the the escape conditions have a strong component outside the ecliptic plane, as clearly visible in Figure 5.5. The  $\varphi$  angle is extremely high in module and in particular is negative. So, according to these data, the escape happens with a latitude close enough to  $-90$  degrees.

Table 5.5: Time comparison between exact and approximate solution

Time	Exact	Approximated
M-M leg	4457,20173	4417,12320
M-escape leg	778,52059	755,36979

Table 5.6: Comparison of orbital parameters between exact and approximate solution, part 1

		a	e	incl
<b>Perigee-FB1</b>	Approximated	300,64615	0,99657	0,50116
	Exact	230,45124	0,99561	0,49854
<b>FB1-FB2</b>	Approximated	88,80794	0,56617	1,78919
	Exact	88,35287	0,64325	1,77504
<b>FB2-ESCAPE</b>	Approximated	-70,00101	1,80220	1,32066
	Exact	-65,97308	1,81739	1,35454

**Table 5.7: Comparison of orbital parameters between exact and approximate solution, part 2**

		<b>RA</b>	<b>w</b>	<b>TA</b>
<b>Perigee-FB1</b>	Approximated	5,51959	5,44057	6,28318
	Exact	0,32075	4,39435	2,83429
<b>FB1-FB2</b>	Approximated	1,44715	5,16438	1,57066
	Exact	1,37996	5,05481	-3,12409
<b>FB2-ESCAPE</b>	Approximated	1,22166	3,12853	1,56878
	Exact	1,16179	3,22493	1,14145

The most important orbital parameters for our study are certainly the semi-major axis, the eccentricity and the inclination. All these 3 values are about constant from one model to another. Moreover, only the final leg turns out to be a hyperbolic orbit (for obvious reasons), while the previous two are elliptic.

But, it can be seen that the semi-major axis from the first to the second leg decreases, with the consequent reduction of energy. The importance of the first flyby is to achieve the right inclination (from 0,5 to 1,78 radians) o then the right trajectory. The second flyby, then is the one that significantly increases the energy.

**Table 5.8: Energy comparison between exact and approximate solution**

		<b>Energy</b>
<b>Perigee-FB1</b>	Approximated	-0,00166
	Exact	-0,00217
<b>FB1-FB2</b>	Approximated	-0,00563
	Exact	-0,00566
<b>FB2-ESCAPE</b>	Approximated	0,00714
	Exact	0,00758

Energy values varies as said before, and as can be clearly seen from the table.

In particular, all the following figures have the equatorial plane as their XY plane and the reference is centered in the centre of mass of the Earth. Therefore, a geocentric reference system is being used. In fact, it can be seen that Moon's orbit is inclined with respect to the ecliptic.

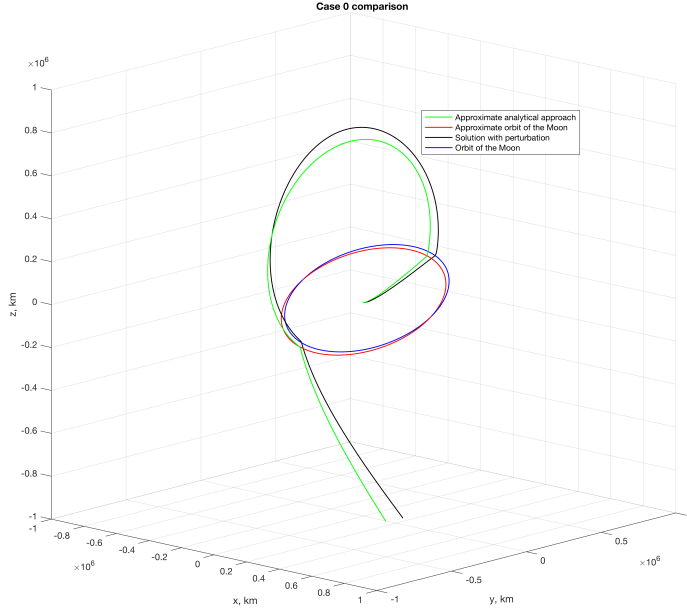


Figure 5.5: Comparison between exact and approximate solution, Case 0

### 5.3 Comparison between solutions with the same escape date

In this section the solutions with the same escape date are compared with each other.

Table 5.9: Comparison of S/C-Moon positions at the two flybys between solutions with the same escape date

Parameter		Case 0	Case 2	Case 4	
<b>FB1</b>	r	S/C	60,56857	60,56831	60,56609
		Moon	60,33634	60,33633	60,33633
	$\vartheta$	S/C	1,34469	1,41183	1,47594
		Moon	1,34238	1,40951	1,47361
	$\varphi$	S/C	0,43526	0,44515	0,45290
		Moon	0,44035	0,44994	0,45738
<b>FB2</b>	r	S/C	60,04843	60,07686	60,10411
		Moon	60,33634	60,33633	60,33633
	$\vartheta$	S/C	4,48059	4,54773	4,61188
		Moon	4,48397	4,55111	4,61520
	$\varphi$	S/C	-0,43773	-0,44747	-0,45508
		Moon	-0,44035	-0,44994	-0,45738

The first thing you notice, as already mentioned, is that with the approximate solutions the distances of the Moon from the Earth at both flybys is the same (about 384400 km, that is, the average Moon-Earth distance) because Moon’s orbit is circular. Whereas, these distances, due to the eccentricity of Moon’s orbit, vary a lot, from a minimum value of about 360000 km to a maximum value of 410000 km.

Another aspect to consider are the angular positions (both of the S/C and of the Moon) that vary from one case to another,

- $\vartheta$ : as can be seen, at both flybys, grows from case 0 to 4 (this indicates that the two flybys occur in successive moments with respect to case 0);
- $\varphi$ : grows from case 0 to 4 at the first flyby (when the Moon is intercepted it is at a higher latitude, compared to the geocentric reference), while at the second one decreases;
- The variation of  $\vartheta$  is one order of magnitude greater than that of  $\varphi$ .

**Table 5.10: Comparison of relative positions at the two flybys between solutions with the same escape date**

	Parameter	Case 0	Case 2	Case 4
<b>FB1</b>	$\vartheta_{SC}-\vartheta_M$	0,002312319	0,00232	0,00233
	$\varphi_{SC}-\varphi_M$	-0,005092084	-0,00479	-0,00448
	$r_{\text{periselenium}}$	0,4059	0,39204	0,37690
	$r_{\text{periselenium}}$ [km]	2588,885524	2500,46514	2403,91321
<b>FB2</b>	$\vartheta_{SC}-\vartheta_M$	-0,003376191	-0,00338	-0,00333
	$\varphi_{SC}-\varphi_M$	0,002615465	0,00246	0,00230
	$r_{\text{periselenium}}$	0,3762	0,35054	0,32481
	$r_{\text{periselenium}}$ [km]	2399,454876	2235,78593	2071,68764

For what concern about the relative angular positions between S/C and Moon at both flybys, they can be summarized as:

- At the first flyby the spacecraft is later ( $\vartheta$ ) and lower ( $\varphi$ ) than the Moon;
- At the second flyby, contrary to what happens to the first one, the spacecraft is more backward ( $\vartheta$ ) and higher ( $\varphi$ ) than the Moon.

The knowledge of these mutual positions was fundamental in order to calculate the exact numerical solution. Only with this exact angular configuration it was possible to obtain the searched solution.

Table 5.11: Comparison of S/C positions between solutions with the same escape date

	Parameter	Case 0	Case 2	Case 4
<b>Perigee</b>	r	1,03020	1,03024	1,03024
	$\vartheta$	-1,54073	-1,46317	-1,39009
	$\varphi$	-0,36676	-0,37910	-0,38550
<b>FB1</b>	r	60,56857	60,56831	60,56609
	$\vartheta$	1,34469	1,41183	1,47594
	$\varphi$	0,43526	0,44515	0,45290
<b>FB2</b>	r	60,04843	60,07686	60,10411
	$\vartheta$	4,48059	4,54773	4,61188
	$\varphi$	-0,43773	-0,44747	-0,45508
<b>Escape</b>	r	156,78561	156,78561	156,78561
	$\vartheta$	-0,41	-0,33177	-0,26772
	$\varphi$	-1,32022	-1,29728	-1,27605

It can be noted that the escape conditions seen at the beginning of this chapter (Table 5.1) are not the same as those in the previous table (Table 5.11). This happens only because they are expressed in two different reference systems: with the appropriate conversions they would coincide.

Table 5.12: Time comparison between solutions with the same escape date

Time	Case 0	Case 2	Case 4
<b>M-M leg</b>	4417,12320	4417,12320	4417,12320
<b>M-escape leg</b>	755,36979	730,07960	706,15763

The previous table (Table 5.12) shows the duration of the Moon to Moon and the Moon to escape legs: you immediately notice that the first leg has the same duration in all 3 cases while the second one decreases its duration. The explanation is that, as shown in the figure below (Figure 5.6), the second flyby of case 4 takes place in a position closer to the escape condition than the other 2 cases. For this reason it is less the time to reach the boundary of the Earth's sphere of influence.

**Table 5.13: Comparison of orbital parameters between solutions with the same escape date, part 1**

		<b>a</b>	<b>e</b>	<b>incl</b>
<b>Perigee-FB1</b>	Case 0	300,64615	0,99657	0,50116
	Case 2	640,87874	0,99839	0,49922
	Case 4	-2938,48377	1,00035	0,50305
<b>FB1-FB2</b>	Case 0	88,80794	0,56617	1,78919
	Case 2	88,80536	0,56616	1,80714
	Case 4	88,79413	0,56612	1,83020
<b>FB2-ESCAPE</b>	Case 0	-70,00101	1,80220	1,32066
	Case 2	-60,95783	1,92457	1,29743
	Case 4	-53,74224	2,05185	1,27611

**Table 5.14: Comparison of orbital parameters between solutions with the same escape date, part 2**

		<b>RA</b>	<b>w</b>	<b>TA</b>
<b>Perigee-FB1</b>	Case 0	5,51959	5,44057	6,28318
	Case 2	5,63918	5,39956	6,28318
	Case 4	5,72239	5,38858	6,28318
<b>FB1-FB2</b>	Case 0	1,44715	5,16438	1,57066
	Case 2	1,52610	5,17628	1,57070
	Case 4	1,60460	5,18687	1,57080
<b>FB2-ESCAPE</b>	Case 0	1,22166	3,12853	1,56878
	Case 2	1,27369	3,15889	1,54414
	Case 4	1,32361	3,18454	1,52188

Talking about orbital parameters, the biggest difference can be seen in the calculation of the semi-major axis for the Perigee-FB1 leg. The main problem you have is in case 4, where the solution gives a negative semi-major axis (hyperbolic orbit), while in the other cases a positive value is obtained (which refers to an elliptical orbit). According to what has just been said, the eccentricity is greater than or less than 1 with minimal differences from the unit.

One of the most important parameters, the inclination between the two flybys, remains almost unchanged (the maximum difference is two degrees). As it happens in the other 2 legs. It can be noted that the initial inclination, about 0,5 radians (approximately 28 degrees), it's the maximum angle between Moon's orbit and Earth's equator.

Table 5.15: Energy comparison between solutions with the same escape date

Energy	Case 0	Case 2	Case 4
<b>Perigee-FB1</b>	-0,00166	-0,00078	0,00017
<b>FB1-FB2</b>	-0,00563	-0,00563	-0,00563
<b>FB2-ESCAPE</b>	0,00714	0,00820	0,00930

The values of energy vary in magnitude by an insignificant factor. As expected, the values in the FB2-escape leg is positive which means that the trajectory is hyperbolic (as can be seen also in the tables with the orbital parameters, in the fb2-escape leg) and therefore you have a hyperbolic excess velocity.

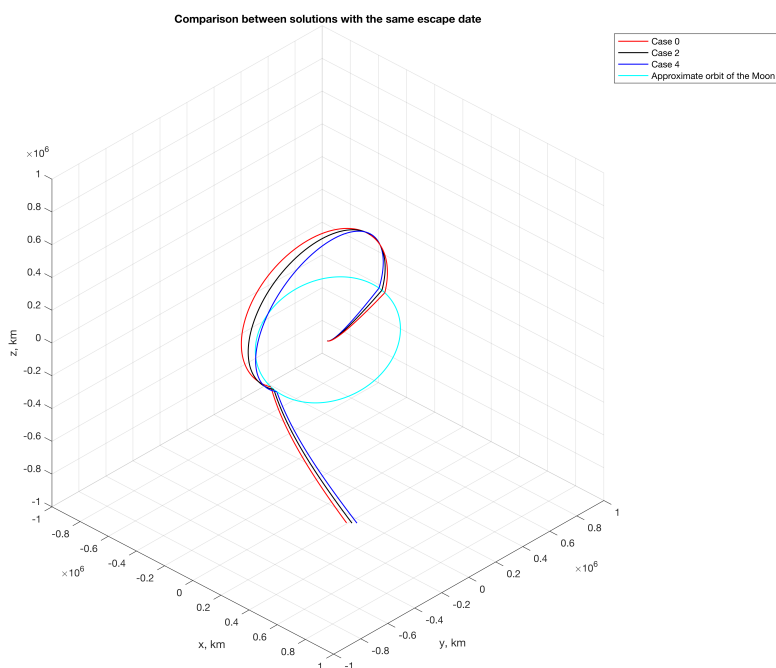


Figure 5.6: Comparison between solutions with the same escape date

## 5.4 Comparison between solutions with the same $V_\infty$

In this section the solutions with the same  $V_\infty$  are compared with each other and with that of the case 0.

**Table 5.16: Comparison of S/C-Moon positions at the two flybys between solutions with the same  $V_\infty$** 

Parameter		Case 0	Case 4	Case 5	Case 6	
<b>FB1</b>	r	S/C	60,56857	60,56609	60,64891	60,84856
		Moon	60,33634	60,33633	60,43736	60,64968
	$\vartheta$	S/C	1,34469	1,47594	1,03329	0,66144
		Moon	1,34238	1,47361	1,03033	0,65828
	$\varphi$	S/C	0,43526	0,45290	0,36798	0,23709
		Moon	0,44035	0,45738	0,37159	0,23950
<b>FB2</b>	r	S/C	60,04843	60,10411	60,21413	60,46568
		Moon	60,33634	60,33633	60,43736	60,64968
	$\vartheta$	S/C	4,48059	4,61188	4,16885	3,79767
		Moon	4,48397	4,61520	4,17192	3,79988
	$\varphi$	S/C	-0,43773	-0,45508	-0,36783	-0,23490
		Moon	-0,44035	-0,45738	-0,37159	-0,23950

Contrary to what happened to the escape with the same date, in this case the value of  $\vartheta$  at both flybys and  $\varphi$  at the first one, decreases significantly by anticipating the escape. Recalling that, the escape of case 6 occurs before the one of case 5, which in turn has earlier escape with respect to case 4. At the second flyby, the value of  $\varphi$ , in antithesis with the previous study, grows.

**Table 5.17: Comparison of relative positions at the two flybys between solutions with the same  $V_\infty$** 

Parameter		Case 0	Case 4	Case 5	Case 6
<b>FB1</b>	$\vartheta_{SC}-\vartheta_M$	0,002312319	0,00233	0,00296	0,00316
	$\varphi_{SC}-\varphi_M$	-0,005092084	-0,00448	-0,00361	-0,00241
	$r_{\text{periselenium}}$	0,4059	0,37690	0,34707	0,30932
	$r_{\text{periselenium}}$ [km]	2588,885524	2403,91321	2213,68900	1972,89432
<b>FB2</b>	$\vartheta_{SC}-\vartheta_M$	-0,003376191	-0,00333	-0,00307	-0,00221
	$\varphi_{SC}-\varphi_M$	0,002615465	0,00230	0,00376	0,00460
	$r_{\text{periselenium}}$	0,3762	0,32481	0,36216	0,35831
	$r_{\text{periselenium}}$ [km]	2399,454876	2071,68764	2309,91443	2285,33479

For what concern about the relative angular positions between S/C and Moon at both flybys, they vary in magnitude but not in sign between all the 5 cases.

So, the reciprocal positions are fixed to obtain this type of trajectory.

Table 5.18: Comparison of S/C positions between solutions with the same  $V_\infty$

	Parameter	Case 0	Case 4	Case 5	Case 6
<b>Perigee</b>	r	1,03020	1,03024	1,03024	1,03024
	$\vartheta$	-1,54073	-1,39009	-1,84844	-2,22219
	$\varphi$	-0,36676	-0,38550	-0,26785	-0,10829
<b>FB1</b>	r	60,56857	60,56609	60,64891	60,84856
	$\vartheta$	1,34469	1,47594	1,03329	0,66144
	$\varphi$	0,435265	0,45290	0,36798	0,23709
<b>FB2</b>	r	60,04843	60,10411	60,21413	60,46568
	$\vartheta$	4,48059	4,61188	4,16885	3,79767
	$\varphi$	-0,43773	-0,45508	-0,36783	-0,23490
<b>Escape</b>	r	156,78561	156,78561	156,78561	156,78561
	$\vartheta$	-0,41	-0,26772	-0,15988	2,16739
	$\varphi$	-1,32022	-1,27605	-1,48478	-1,43163

Table 5.19: Time comparison between solutions with the same  $V_\infty$

Time	Case 0	Case 4	Case 5	Case 6
M-M leg	4417,12320	4417,12320	4428,22166	4451,57664
M-escape leg	755,36979	706,15763	748,44815	779,77558

In this case, even the M-M leg varies its duration increasing it, while the M-escape leg becomes shorter.

Table 5.20: Comparison of orbital parameters between solutions with the same  $V_\infty$ , part 1

		a	e	incl
<b>Perigee-FB1</b>	Case 0	300,64615	0,99657	0,50116
	Case 4	-2938,48377	1,00035	0,50305
	Case 5	-472,11528	1,00218	0,50501
	Case 6	-136,47187	1,00754	0,50274
<b>FB1-FB2</b>	Case 0	88,80794	0,56617	1,78919
	Case 4	88,79413	0,56612	1,83020
	Case 5	88,95768	0,56620	2,08356
<b>FB2-ESCAPE</b>	Case 6	89,26654	0,566157	2,40302
	Case 0	-70,00101	1,80220	1,32066
	Case 4	-53,74224	2,05185	1,27611
	Case 5	-53,74761	2,09924	1,49193
	Case 6	-53,74261	2,121569	1,70933

**Table 5.21: Comparison of orbital parameters between solutions with the same  $V_\infty$ , part 2**

		<b>RA</b>	<b>w</b>	<b>TA</b>
<b>Perigee-FB1</b>	Case 0	5,51959	5,44057	6,28318
	Case 4	5,72239	5,38858	6,28318
	Case 5	4,95423	5,70438	0,00001
	Case 6	4,26003	6,05695	6,28318
<b>FB1-FB2</b>	Case 0	1,44715	5,16438	1,57066
	Case 4	1,60460	5,18687	1,57080
	Case 5	1,25153	5,14225	1,57074
	Case 6	0,92981	5,07259	1,57068
<b>FB2-ESCAPE</b>	Case 0	1,22166	3,12853	1,56878
	Case 4	1,32361	3,18454	1,52188
	Case 5	0,99950	3,25602	1,49074
	Case 6	0,69236	3,24931	1,47635

The semi-major axis of the first leg, in the last 3 cases, remains negative while the eccentricity grows a little. In the same way, even the inclination of the second leg grows a lot, with a margin of about 35 degrees. All these considerations can be seen in the figure below (Figure 5.7).

Moreover, it can be notice that changing the escape date (cases 5 and 6) varies considerably the Perigee-Moon leg: in fact, in cases 0 2 and 4 (considering the solution which takes into account perturbations) this leg is elliptical while, in the other 2 cases, orbit is hyperbolic.

**Table 5.22: Energy comparison between solutions with the same  $V_\infty$**

<b>Energy</b>	<b>Case 0</b>	<b>Case 4</b>	<b>Case 5</b>	<b>Case 6</b>
<b>Perigee-FB1</b>	-0,00166	0,00017	0,00106	0,00366
<b>FB1-FB2</b>	-0,00563	-0,00563	-0,00562	-0,0056
<b>FB2-ESCAPE</b>	0,00714	0,00930	0,00930	0,00930

In this case, the final energy maintains the same value that is still greater than the reference case (case 0), because, compared to it, the final leg has greater semi-major axis as well as  $V_\infty$ .

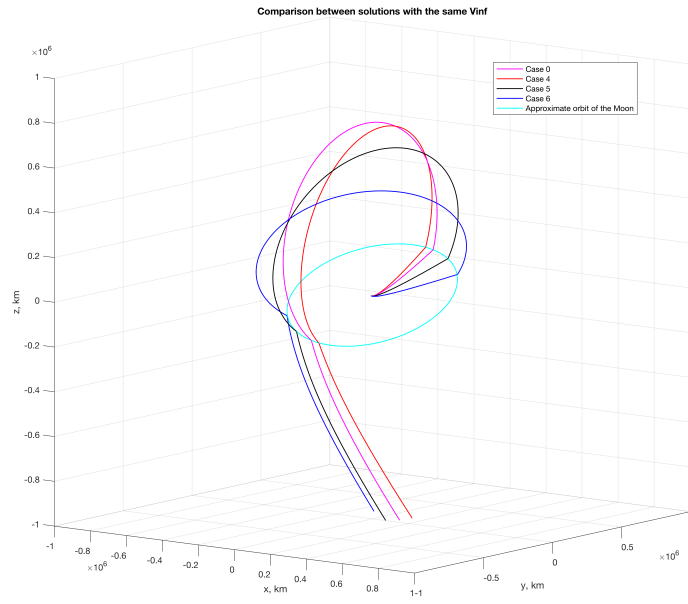


Figure 5.7: Comparison between solutions with the same  $V_{\infty}$

## Chapter 6

# Exact numerical solution results

In the following chapter, will be presented the exact numerical solutions. Then, they are compared with the approximate ones (without perturbations), keeping the same escape conditions (Table 5.1).

### 6.1 Comparison between solutions with the same escape date

Table 6.1: Mass and times as the  $V_\infty$  varies

Case	0	2	4
Mass [kg]	10318,06402	10310,76261	10301,86671
Mass correct [kg]	9768,06402	9760,76261	9751,86671
$V_\infty$	1,3	1,35	1,4
T1	255,87464	254,22257	252,00386
T2	2457,49223	2452,95069	2449,59207
T2	4713,07637	4704,69311	4696,55410
T3	5491,59696	5454,88856	5420,41797
Date of FB1	30/4/2022	1/5/2022	1/5/2022
Date of apogee	3/5/2022	3/5/2022	3/5/2022
Date of FB2	13/6/2022	14/6/2022	14/6/2022
Date of escape	21/6/2022	21/6/2022	21/6/2022

It can be noticed immediately that, increasing  $V_\infty$  the mass at the escape is a bit lower. In the same way varies the time needed to reach the boundary of the sphere of influence.

In particular, most of the time is occupied from the first flyby to the second one (about the 80% of the total flight time).

Table 6.2: Comparison of the periselenium radius at the 2 flybys

Case		0	2	4
$r_{\text{periselenium}}$ <b>FB1</b> [km]		3072,78235	3014,73755	2937,70777
$r_{\text{periselenium}}$ <b>FB2</b> [km]		2845,37283	2633,72663	2425,86125

The distances of the spacecraft at both flybys decreases as  $V_{\infty}$  increases, in particular that relating to the second one.

Table 6.3: Comparison of S/C-Moon positions at the two flybys

	Case	0	2	4	
<b>FB1</b>	r	S/C	64,30885577	64,37878	64,42534
		Moon	64,02390329	64,09538	64,14464
	$\vartheta$	S/C	1,26702922	1,33862	1,40507
		Moon	1,26451688	1,33617	1,40266
	$\varphi$	S/C	0,42131895	0,43392	0,44380
		Moon	0,42692323	0,43937	0,44904
$r_{\text{periselenium}}$		0,48176806	0,47267	0,46059	
$r_{\text{periselenium}}$ [km]		3072,78234	3014,73757	2937,70780	
<b>FB2</b>	r	S/C	56,26755091	56,24613	56,24091
		Moon	56,59548797	56,54160	56,50561
	$\vartheta$	S/C	4,418746267	4,49328	4,56346
		Moon	4,423174	4,49765	4,56771
	$\varphi$	S/C	-0,4265	-0,43921	-0,44906
		Moon	-0,43007	-0,44245	-0,45203
$r_{\text{periselenium}}$		0,4461135243	0,41293	0,38034	
$r_{\text{periselenium}}$ [km]		2845,37286	2633,72663	2425,86123	

As shown in the figure below (Figure 6.1 and 6.2), the 3 trajectories are very similar to each other, but slightly rotated forward with respect to each other: if the values of  $\varphi$  vary a little,  $\vartheta$  grows much more.

Table 6.4: Adimensional spherical coordinates of the S/C in points of particular interest as the  $V_\infty$  varies

	Case	0	2	4
<b>Perigee</b>	r	1,03020	1,03020	1,03020
	$\vartheta$	-1,60680	-1,52940	-1,45690
	$\varphi$	-0,47	-0,47850	-0,48420
<b>FB1</b>	r	64,30886	64,37878	64,42534
	$\vartheta$	1,26703	1,33862	1,40507
	$\varphi$	0,42132	0,43392	0,44380
<b>Apogee</b>	r	145,18130	144,99180	144,81540
	$\vartheta$	-1,24720	-1,18670	-1,11560
	$\varphi$	1,17240	1,16130	1,14670
<b>FB2</b>	r	56,26755	56,24613	56,24091
	$\vartheta$	4,418746267	-1,78991	-1,71973
	$\varphi$	-0,4265	-0,43921	-0,44906
<b>Escape</b>	r	156,7856	156,78560	156,78560
	$\vartheta$	0,0314	0,03540	0,04470
	$\varphi$	-1,3333	-1,30850	-1,28620

An important aspect that can be seen here, are the escape conditions: as already mentioned, the first 3 cases only differ for the escape velocity magnitude. Thus, asymptotically they have the same trajectory: the 3 lines, after the second flyby, are getting closer and closer as they approach the boundary of the sphere of influence, Figure 6.1.

**Table 6.5:** Adimensional velocities of the S/C in points of particular interest as the  $V_\infty$  varies

	Case	0	2	4
<b>Perigee</b>	u	0	0	0
	v	1,37240	1,37810	1,38260
	w	-0,23120	-0,19620	-0,16510
<b>FB1</b>	u	0,19670	0,19870	0,20110
	v	-0,08760	-0,08730	-0,08800
	w	0,09520	0,09700	0,09870
<b>Apogee</b>	u	0	0	0
	v	-0,02580	-0,02510	-0,02500
	w	-0,04230	-0,04300	-0,04330
<b>FB2</b>	u	-0,01240	-0,01140	-0,01050
	v	-0,06550	-0,06320	-0,06220
	w	-0,2698	-0,27860	-0,28770
<b>Escape</b>	u	0,1452	0,15150	0,15780
	v	0,0704	0,07350	0,07630
	w	0,0317	0,02830	0,02540

As it should be, both at the perigee (departure of our trajectory) and at the apogee, the radial velocity (u) is zero.

**Table 6.6:** Initial and final semi-axis and energy

Case	0	2	4
<b>Initial semi-axis</b>	231,72704	283,06109	387,81870
<b>Final semi-axis</b>	-69,99874	-60,95273	-53,74490
<b>Final energy</b>	0,00714	0,00820	0,00930

Due to an increment on the final semi-major axis (in magnitude it is reduced), the final energy grows.

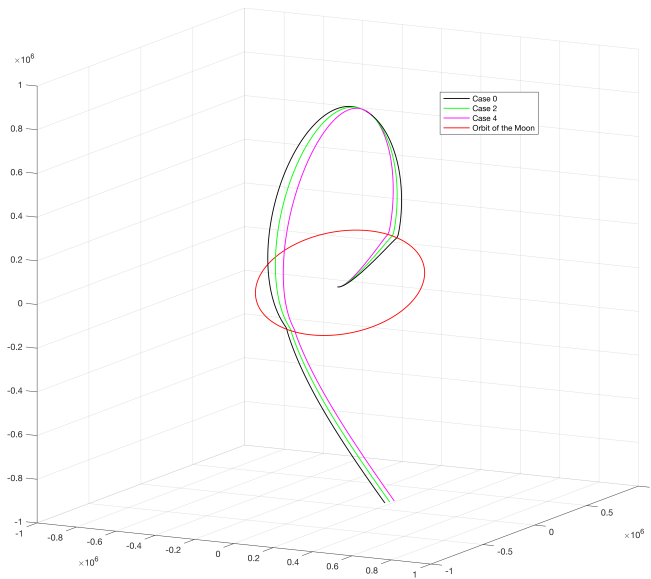


**Figure 6.1:** Comparison between solutions as the  $V_\infty$  varies, 3D view

In this view (Figure 6.1, in which it is possible to have a 3-dimensional view of the entire trajectory), you can realize that the Moon-Moon leg is obtained through a retrograde orbit (inclination greater than 90 degrees).

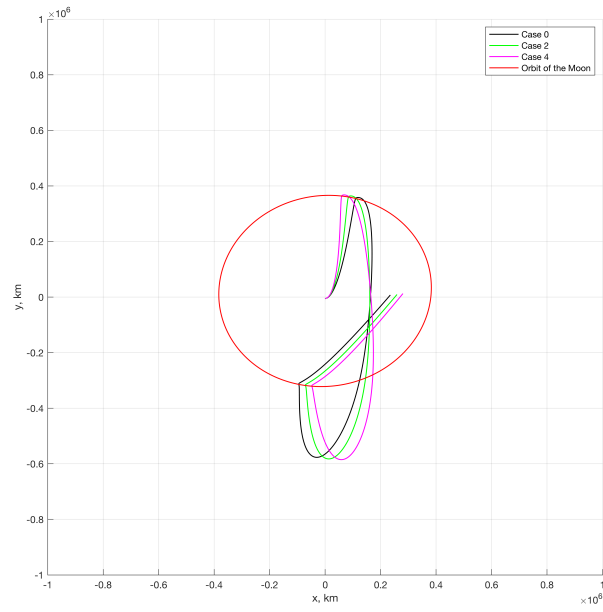


Figure 6.2: Comparison between solutions as the  $V_\infty$  varies, XY view

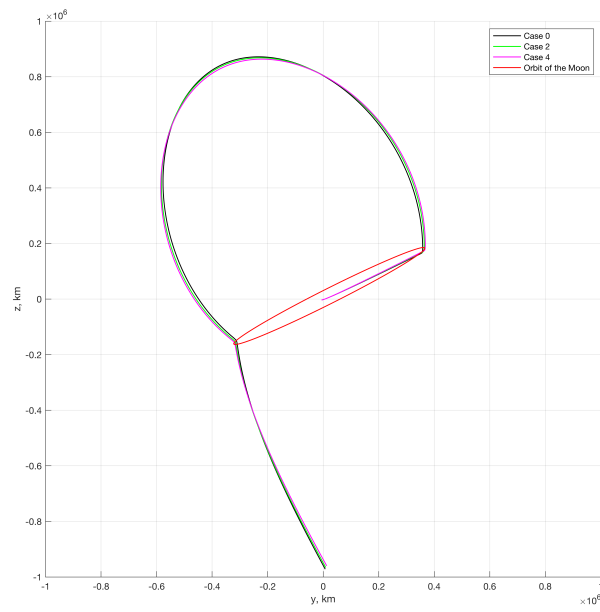


Figure 6.3: Comparison between solutions as the  $V_\infty$  varies, YZ view

## 6.2 Comparison between solutions with the same $V_\infty$

Table 6.7: Mass and times as the date of escape varies

Case	0	4	5	6
Mass [kg]	10318,06402	10301,86671	10246,20564	10163,21690
Mass correct [kg]	9768,06402	9751,86671	9696,20564	9613,21690
$V_\infty$	1,3	1,4	1,4	1,4
T1	255,87464	252,00386	236,59710	216,06620
T2	2457,49223	2449,59207	2466,66770	2455,65680
T2	4713,07637	4696,55410	4742,98600	4801,47600
T3	5491,59696	5420,41797	5505,84100	5592,87430
Date of FB1	30/4/2022	1/5/2022	29/4/2022	27/4/2022
Date of apogee	3/5/2022	3/5/2022	1/5/2022	29/4/2022
Date of FB2	13/6/2022	14/6/2022	12/ 6/2022	11/ 6/2022
Date of escape	21/6/2022	21/6/2022	19/ 6/2022	18/ 6/2022

Talking about the flight time, it seems that the last case is the longest, although the duration of all the transfers is very similar and on average it takes about 53 days.

Table 6.8: Comparison of the periselenium radius at the 2 flybys

Case	0	4	5	6
$r_{\text{periselenium}}$ FB1 [km]	3072,78235	2937,70777	2451,39282	2058,06497
$r_{\text{periselenium}}$ FB2 [km]	2845,37283	2425,86125	2595,54766	2504,02244

Table 6.9: Comparison of S/C-Moon positions at the two flybys

		Case	0	4	5	6
<b>FB1</b>	r	S/C	64,30885577	64,42534	64,11500	63,18250
		Moon	64,02390329	64,14464	63,86302	62,95801
	$\vartheta$	S/C	1,26702922	1,40507	0,97670	0,59560
		Moon	1,26451688	1,40266	0,97355	0,59234
	$\varphi$	S/C	0,42131895	0,44380	0,35140	0,20930
		Moon	0,42692323	0,44904	0,35484	0,21108
	$r_{\text{periselenium}}$		0,48176806	0,46059	0,38434	0,32267
	$r_{\text{periselenium}}$ [km]		3072,78234	2937,70780	2451,39280	2058,06496
<b>FB2</b>	r	S/C	56,26755091	56,24091	56,56920	57,56510
		Moon	56,59548797	56,50561	56,80579	57,74568
	$\vartheta$	S/C	4,418746267	4,56346	4,13269	3,77159
		Moon	4,423174	4,56771	4,13647	3,77433
	$\varphi$	S/C	-0,4265	-0,44906	-0,35670	-0,22320
		Moon	-0,43007	-0,45203	-0,36128	-0,22865
	$r_{\text{periselenium}}$		0,4461135243 3	0,38034	0,40694	0,39259
	$r_{\text{periselenium}}$ [km]		2845,37286	2425,86123	2595,54766	2504,02244

It can be noted that the distance of the Moon from the Earth at flybys is different: it is farther at the first one, and overall the difference of radius is about 50000 km. This happens because it is considered the eccentricity of Moon's orbit, which did not happen in the approximate approach.

Table 6.10: Adimensional spherical coordinates of the S/C in points of particular interest as the date of escape varies

	Case	0	4	5	6
<b>Perigee</b>	r	1,03020	1,03020	1,03020	1,03020
	$\vartheta$	-1,60680	-1,45690	-1,87860	-2,25250
	$\varphi$	-0,47	-0,48420	-0,43210	-0,33190
<b>FB1</b>	r	64,30886	64,42534	64,11500	63,18250
	$\vartheta$	1,26703	1,40507	0,97670	0,59560
	$\varphi$	0,42132	0,44380	0,35140	0,20930
<b>Apogee</b>	r	145,18130	144,81540	146,64740	148,83120
	$\vartheta$	-1,24720	-1,11560	-0,98700	-0,98710
	$\varphi$	1,17240	1,14670	0,96820	0,68700
<b>FB2</b>	r	56,26755	56,24091	56,56920	57,56510
	$\vartheta$	4,418746267	-1,71973	4,13269	3,77159
	$\varphi$	-0,4265	-0,44906	-0,35670	-0,22320
<b>Escape</b>	r	156,7856	156,78560	156,78560	156,78560
	$\vartheta$	0,0314	0,04470	0,57250	1,69739
	$\varphi$	-1,3333	-1,28620	-1,43320	-1,38430

Table 6.11: Adimensional velocities of the S/C in points of particular interest as the date of escape varies

	Case	0	4	5	6
<b>Perigee</b>	u	0	0	0	0
	v	1,37240	1,38260	1,34950	1,29930
	w	-0,23120	-0,16510	-0,35130	-0,35130
<b>FB1</b>	u	0,19670	0,20110	0,21820	0,24100
	v	-0,08760	-0,08800	-0,12540	-0,15360
	w	0,09520	0,09870	0,07570	0,04100
<b>Apogee</b>	u	0	0	0	0
	v	-0,02580	-0,02500	-0,04230	-0,04740
	w	-0,04230	-0,04330	-0,02400	-0,00710
<b>FB2</b>	u	-0,01240	-0,01050	-0,02950	-0,03980
	v	-0,06550	-0,06220	-0,12210	-0,17810
	w	-0,2698	-0,28770	-0,25820	-0,22040
<b>Escape</b>	u	0,1452	0,15780	0,15660	0,15550
	v	0,0704	0,07630	0,03170	-0,07340
	w	0,0317	0,02540	0,07640	0,04250

Table 6.12: Initial and final semi-axis and energy

Case	0	4	5	6
Initial semi-axis	231,72704	387,81870	-293,13240	-80,62070
Final semi-axis	-69,99874	-53,74490	-53,74515	-53,74510
Final energy	0,00714	0,00930	0,00930	0,00930

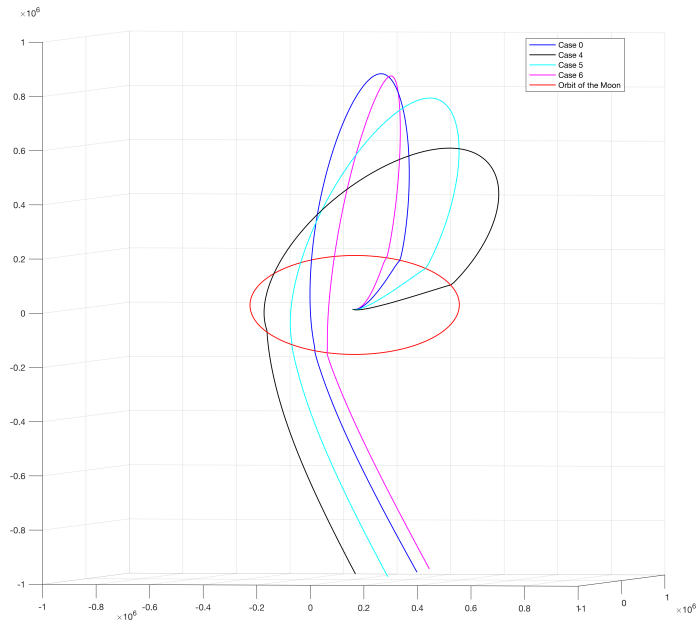


Figure 6.4: Comparison between solutions as the escape date varies, 3D view

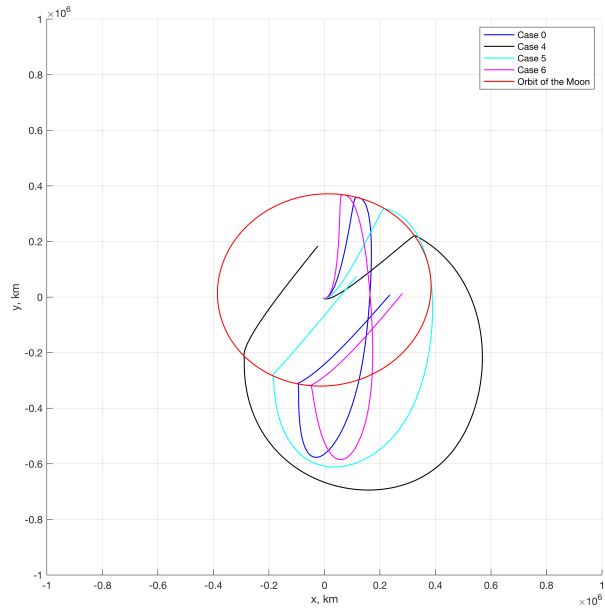


Figure 6.5: Comparison between solutions as the escape date varies, XY view

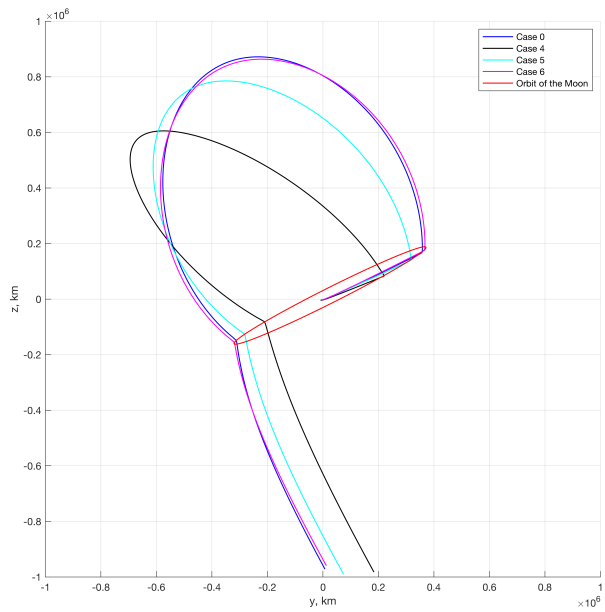


Figure 6.6: Comparison between solutions as the escape date varies, YZ view

### 6.3 Comparison between exact and approximated solutions

In this section the results of the remaining 4 cases are reported and each of them is compared to the solution without perturbations.

#### 6.3.1 Case 2

The same conclusions obtained previously (Section 6.1), can be even obtained from the following tables and figures.

**Table 6.13: Comparison of S/C-Moon positions at the two flybys between exact and approximate solution**

Parameter		Exact	Approximated
<b>FB1</b>	r	S/C	64,37878
		Moon	60,56831
	$\vartheta$	S/C	64,09538
		Moon	60,33633
	$\varphi$	S/C	1,33862
		Moon	1,41183
$\varphi$	S/C	1,33617	
	Moon	1,40951	
<b>FB2</b>	r	S/C	0,43392
		Moon	0,44515
	$\vartheta$	S/C	0,43937
		Moon	0,44994
	$\varphi$	S/C	56,24613
		Moon	60,07686
$\vartheta$	S/C	56,54160	
	Moon	60,33633	
$\varphi$	S/C	4,49328	
	Moon	4,54773	
$\varphi$	S/C	4,49765	
	Moon	4,55111	
$\varphi$	S/C	-0,43921	
	Moon	-0,44747	
$\varphi$	S/C	-0,44245	
	Moon	-0,44994	

**Table 6.14: Comparison of relative positions at the two flybys between exact and approximate solution**

Parameter		Exact	Approximated
<b>FB1</b>	$\vartheta_{SC}-\vartheta_M$	0,00245	0,00232
	$\varphi_{SC}-\varphi_M$	-0,00545	-0,00479
	$\Gamma_{\text{periselenium}}$	0,47267	0,39204
	$\Gamma_{\text{periselenium}}$	3014,73755	2500,46514
<b>FB2</b>	$\vartheta_{SC}-\vartheta_M$	-0,00437	-0,00338
	$\varphi_{SC}-\varphi_M$	0,00325	0,00246
	$\Gamma_{\text{periselenium}}$	0,41293	0,35054
	$\Gamma_{\text{periselenium}}$	2633,72663	2235,78593

Probably this table remains one of the key points of the discussion. It is important to underline that the reciprocal positions between S/C and Moon remain unchanged (they only vary in magnitude), both by changing cases and by the model used to derive the solution.

Table 6.15: Comparison of S/C positions between exact and approximate solution

	Parameter	Exact	Approximated
<b>Perigee</b>	r	1,03020	1,03024
	$\vartheta$	-1,52940	-1,46317
	$\varphi$	-0,47850	-0,37910
<b>FB1</b>	r	64,37878	60,56831
	$\vartheta$	1,33862	1,41183
	$\varphi$	0,43392	0,44515
<b>FB2</b>	r	56,24613	60,07686
	$\vartheta$	4,49328	4,54773
	$\varphi$	-0,43921	-0,44747
<b>Escape</b>	r	156,78560	156,78561
	$\vartheta$	0,03540	-0,33177
	$\varphi$	-1,30850	-1,29728

Table 6.16: Time comparison between exact and approximate solution

Time	Exact	Approximated
M-M leg	4450,47054	4417,12320
M-escape leg	750,19545	730,07960

Table 6.17: Comparison of orbital parameters between exact and approximate solution, part 1

		a	e	incl
<b>Perigee-FB1</b>	Approximated	640,87874	0,99839	0,49922
	Exact	279,34356	0,99637	0,49844
<b>FB1-FB2</b>	Approximated	88,80536	0,56616	1,80714
	Exact	88,34860	0,64122	1,77393
<b>FB2-ESCAPE</b>	Approximated	-60,95783	1,92457	1,29743
	Exact	-57,97184	1,92945	1,32632

Table 6.18: Comparison of orbital parameters between exact and approximate solution, part 2

		RA	w	TA
<b>Perigee-FB1</b>	Approximated	5,63918	5,39956	6,28318
	Exact	0,34236	4,44475	2,82777
<b>FB1-FB2</b>	Approximated	1,52610	5,17628	1,57070
	Exact	1,46047	5,06774	-3,11958
<b>FB2-ESCAPE</b>	Approximated	1,27369	3,15889	1,54414
	Exact	1,21928	3,24309	1,15813

Again, it is extremely important the inclination of the FB1-FB2 leg to achieve a backflip transfer and obviously having a hyperbolic solution in the final leg.

Table 6.19: Energy comparison between exact and approximate solution

		Energy
<b>Perigee-FB1</b>	Approximated	-0,00078
	Exact	-0,00179
<b>FB1-FB2</b>	Approximated	-0,00563
	Exact	-0,00566
<b>FB2-ESCAPE</b>	Approximated	0,00820
	Exact	0,00862

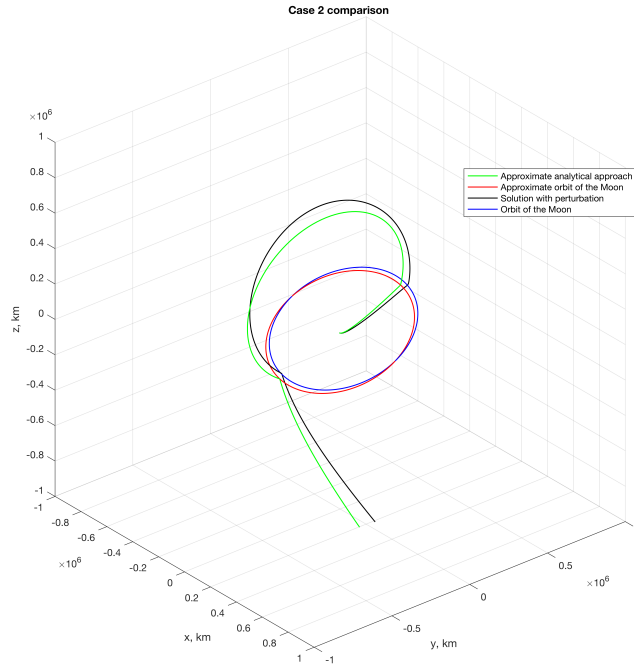


Figure 6.7: Comparison between exact and approximate solution, Case 2

### 6.3.2 Case 4

Table 6.20: Comparison of S/C-Moon positions at the two flybys between exact and approximate solution

Parameter		Exact	Approximated
<b>FB1</b>	r	S/C	64,42534
		Moon	60,33633
	$\vartheta$	S/C	1,40507
		Moon	1,47361
$\varphi$	S/C	0,44380	
	Moon	0,45738	
<b>FB2</b>	r	S/C	56,50561
		Moon	60,33634
	$\vartheta$	S/C	4,56346
		Moon	4,61520
$\varphi$	S/C	-0,44906	
	Moon	-0,45738	

Table 6.21: Comparison of relative positions at the two flybys between exact and approximate solution

	Parameter	Exact	Approximated
<b>FB1</b>	$\vartheta_{SC}-\vartheta_M$	0,00241	0,00233
	$\varphi_{SC}-\varphi_M$	-0,00525	-0,00448
	$r_{\text{periselenium}}$	0,46059	0,37690
	$r_{\text{periselenium}}$	2937,70777	2403,91321
<b>FB2</b>	$\vartheta_{SC}-\vartheta_M$	-0,00425	-0,00333
	$\varphi_{SC}-\varphi_M$	0,00297	0,00230
	$r_{\text{periselenium}}$	0,38034	0,32481
	$r_{\text{periselenium}}$	2425,86125	2071,68764

Table 6.22: Comparison of S/C positions between exact and approximate solution

	Parameter	Exact	Approximated
<b>Perigee</b>	$r$	1,03020	1,03024
	$\vartheta$	-1,52940	-1,39009
	$\varphi$	-0,47850	-0,38550
<b>FB1</b>	$r$	64,37878	60,56609
	$\vartheta$	1,33862	1,47594
	$\varphi$	0,43392	0,45290
<b>FB2</b>	$r$	56,24613	60,10411
	$\vartheta$	4,49328	4,61188
	$\varphi$	-0,43921	-0,45508
<b>Escape</b>	$r$	156,78560	156,78561
	$\vartheta$	0,03540	-0,26772
	$\varphi$	-1,30850	-1,27605

Table 6.23: Time comparison between exact and approximate solution

Time	Exact	Approximated
M-M leg	4444,55024	4417,12320
M-escape leg	723,86387	706,15763

**Table 6.24: Comparison of orbital parameters between exact and approximate solution, part 1**

		<b>a</b>	<b>e</b>	<b>incl</b>
<b>Perigee-FB1</b>	Approximated	-2938,48377	1,00035	0,50305
	Exact	383,49735	0,99736	0,49847
<b>FB1-FB2</b>	Approximated	88,79413	0,56612	1,83020
	Exact	88,35795	0,63905	1,77912
<b>FB2-ESCAPE</b>	Approximated	-53,74224	2,05185	1,27611
	Exact	-51,49384	2,04590	1,30099

The semi-axis of the first leg of this case is certainly the one that, when compared with all cases, differs more between the two types of solution. That is, because in one instance it gives you an elliptical orbit, in the other a hyperbolic one.

**Table 6.25: Comparison of orbital parameters between exact and approximate solution, part 2**

		<b>RA</b>	<b>w</b>	<b>TA</b>
<b>Perigee-FB1</b>	Approximated	5,72239	5,38858	6,28318
	Exact	0,36645	4,48802	2,82557
<b>FB1-FB2</b>	Approximated	1,60460	5,18687	1,57080
	Exact	1,53892	5,08183	-3,11944
<b>FB2-ESCAPE</b>	Approximated	1,32361	3,18454	1,52188
	Exact	1,27380	3,25850	1,17309

**Table 6.26: Energy comparison between exact and approximate solution**

		<b>Energy</b>
<b>Perigee-FB1</b>	Approximated	0,00017
	Exact	-0,00130
<b>FB1-FB2</b>	Approximated	-0,00563
	Exact	-0,00566
<b>FB2-ESCAPE</b>	Approximated	0,00930
	Exact	0,00971

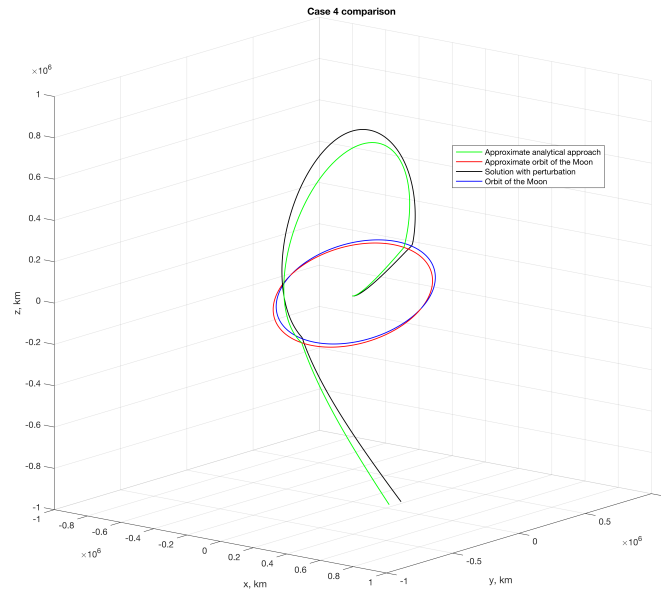


Figure 6.8: Comparison between exact and approximate solution, Case 4

### 6.3.3 Case 5

Table 6.27: Comparison of S/C-Moon positions at the two flybys between exact and approximate solution

		Parameter	Exact	Approximated
<b>FB1</b>	r	S/C	64,11500	60,64891
		Moon	63,86302	60,43736
	$\vartheta$	S/C	0,97670	1,03329
		Moon	0,97355	1,03033
	$\varphi$	S/C	0,35140	0,36798
		Moon	0,35484	0,37159
<b>FB2</b>	r	S/C	56,56920	60,21413
		Moon	56,80579	60,43736
	$\vartheta$	S/C	4,13269	4,16885
		Moon	4,13647	4,17192
	$\varphi$	S/C	-0,35670	-0,36783
		Moon	-0,36128	-0,37159

Table 6.28: Comparison of relative positions at the two flybys between exact and approximate solution

	Parameter	Exact	Approximated
<b>FB1</b>	$\vartheta_{SC}-\vartheta_M$	0,00315	0,00296
	$\varphi_{SC}-\varphi_M$	-0,00344	-0,00361
	$r_{\text{periselenium}}$	0,38434	0,34707
	$r_{\text{periselenium}}$	2451,39281	2213,68900
<b>FB2</b>	$\vartheta_{SC}-\vartheta_M$	-0,00378	-0,00307
	$\varphi_{SC}-\varphi_M$	0,00458	0,00376
	$r_{\text{periselenium}}$	0,40694	0,36216
	$r_{\text{periselenium}}$	2595,54766	2309,91443

Table 6.29: Comparison of S/C positions between exact and approximate solution

	Parameter	Exact	Approximated
<b>Perigee</b>	$r$	1,03020	1,03024
	$\vartheta$	-1,87860	-1,84844
	$\varphi$	-0,43210	-0,26785
<b>FB1</b>	$r$	64,11500	60,64891
	$\vartheta$	0,97670	1,03329
	$\varphi$	0,35140	0,36798
<b>FB2</b>	$r$	56,56920	60,21413
	$\vartheta$	4,13269	4,16885
	$\varphi$	-0,35670	-0,36783
<b>Escape</b>	$r$	156,78560	156,78561
	$\vartheta$	0,57250	-0,15988
	$\varphi$	-1,43320	-1,48478

Table 6.30: Time comparison between exact and approximate solution

Time	Exact	Approximated
M-M leg	4506,38890	4428,22166
M-escape leg	849,88830	748,44815

Table 6.31: Comparison of orbital parameters between exact and approximate solution, part 1

		<b>a</b>	<b>e</b>	<b>incl</b>
<b>Perigee-FB1</b>	Approximated	-472,11528	1,00218	0,50501
	Exact	-300,06129	1,00338	0,49827
<b>FB1-FB2</b>	Approximated	88,95768	0,56620	2,08356
	Exact	88,71392	0,65308	2,08689
<b>FB2-ESCAPE</b>	Approximated	-53,74761	2,09924	1,49193
	Exact	-51,29322	2,09010	1,51855

Table 6.32: Comparison of orbital parameters between exact and approximate solution, part 2

		<b>RA</b>	<b>w</b>	<b>TA</b>
<b>Perigee-FB1</b>	Approximated	4,95423	5,70438	0,00001
	Exact	0,24832	4,21123	2,81070
<b>FB1-FB2</b>	Approximated	1,25153	5,14225	1,57074
	Exact	1,18478	5,03675	-3,12839
<b>FB2-ESCAPE</b>	Approximated	0,99950	3,25602	1,49074
	Exact	0,95839	3,31690	0,99325

Table 6.33: Energy comparison between exact and approximate solution

		<b>Energy</b>
<b>Perigee-FB1</b>	Approximated	0,00106
	Exact	0,00167
<b>FB1-FB2</b>	Approximated	-0,00562
	Exact	-0,00564
<b>FB2-ESCAPE</b>	Approximated	0,00930
	Exact	0,00975

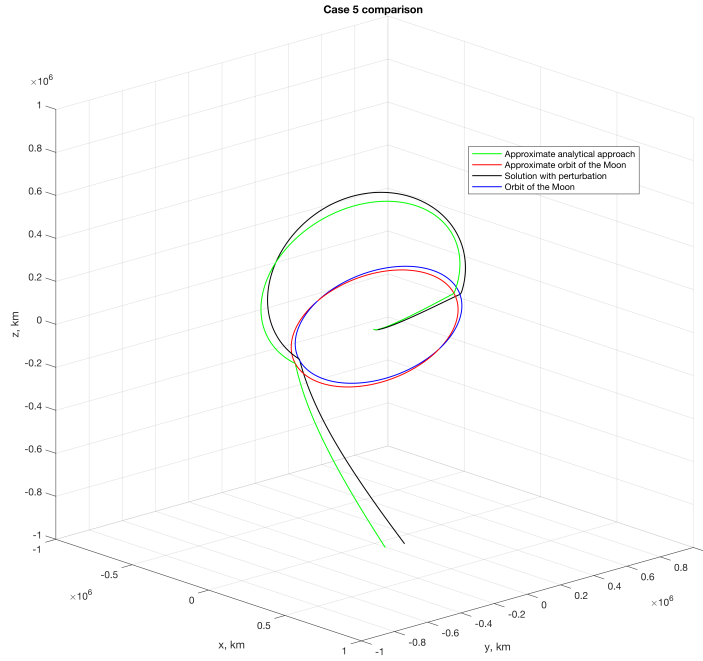


Figure 6.9: Comparison between exact and approximate solution, Case 5

### 6.3.4 Case 6

Table 6.34: Comparison of S/C-Moon positions at the two flybys between exact and approximate solution

Parameter		Exact	Approximated
<b>FB1</b>	r	S/C	63,18250
		Moon	62,95801
	$\vartheta$	S/C	0,59560
		Moon	0,59234
$\varphi$	S/C	0,20930	
	Moon	0,21108	
<b>FB2</b>	r	S/C	57,56510
		Moon	57,74568
	$\vartheta$	S/C	3,77159
		Moon	3,77433
$\varphi$	S/C	-0,22320	
	Moon	-0,22865	

Table 6.35: Comparison of relative positions at the two flybys between exact and approximate solution

	Parameter	Exact	Approximated
<b>FB1</b>	$\vartheta_{SC}-\vartheta_M$	0,00326	0,00316
	$\varphi_{SC}-\varphi_M$	-0,00178	-0,00241
	$r_{\text{periselenium}}$	0,32267	0,30932
	$r_{\text{periselenium}}$	2058,06497	1972,89432
<b>FB2</b>	$\vartheta_{SC}-\vartheta_M$	-0,00275	-0,00221
	$\varphi_{SC}-\varphi_M$	0,00545	0,00460
	$r_{\text{periselenium}}$	0,39259	0,35831
	$r_{\text{periselenium}}$	2504,02244	2285,33479

Table 6.36: Comparison of S/C positions between exact and approximate solution

	Parameter	Exact	Approximated
<b>Perigee</b>	$r$	1,03020	1,03024
	$\vartheta$	-2,25250	-2,22219
	$\varphi$	-0,33190	-0,10829
<b>FB1</b>	$r$	63,18250	60,84856
	$\vartheta$	0,59560	0,66144
	$\varphi$	0,20930	0,23709
<b>FB2</b>	$r$	57,56510	60,46568
	$\vartheta$	3,77159	3,79767
	$\varphi$	-0,22320	-0,23490
<b>Escape</b>	$r$	156,78560	156,78561
	$\vartheta$	1,69739	2,16739
	$\varphi$	-1,38430	-1,43163

Table 6.37: Time comparison between exact and approximate solution

Time	Exact	Approximated
M-M leg	4585,40980	4451,57664
M-escape leg	791,39830	779,77558

Table 6.38: Comparison of orbital parameters between exact and approximate solution, part 1

		<b>a</b>	<b>e</b>	<b>incl</b>
<b>Perigee-FB1</b>	Approximated	-136,4718737	1,007549109	0,502741029
	Exact	-81,57112353	1,01240796	0,49824355
<b>FB1-FB2</b>	Approximated	89,26654297	0,566157657	2,403023381
	Exact	89,81218254	0,65722618	2,44155830
<b>FB2-ESCAPE</b>	Approximated	-53,74261137	2,121569165	1,709328516
	Exact	-51,22076875	2,12232135	1,73264129

Table 6.39: Comparison of orbital parameters between exact and approximate solution, part 2

		<b>RA</b>	<b>w</b>	<b>TA</b>
<b>Perigee-FB1</b>	Approximated	4,26003	6,05695	6,28318
	Exact	0,20047	3,89262	2,79412
<b>FB1-FB2</b>	Approximated	0,92981	5,07259	1,57068
	Exact	0,81271	4,88578	-3,12340
<b>FB2-ESCAPE</b>	Approximated	0,69236	3,24931	1,47635
	Exact	0,65587	3,30008	0,77187

Table 6.40: Energy comparison between exact and approximate solution

		<b>Energy</b>
<b>Perigee-FB1</b>	Approximated	0,003663759
	Exact	0,00612962
<b>FB1-FB2</b>	Approximated	-0,005601203
	Exact	-0,005567173
<b>FB2-ESCAPE</b>	Approximated	0,009303604
	Exact	0,009761665

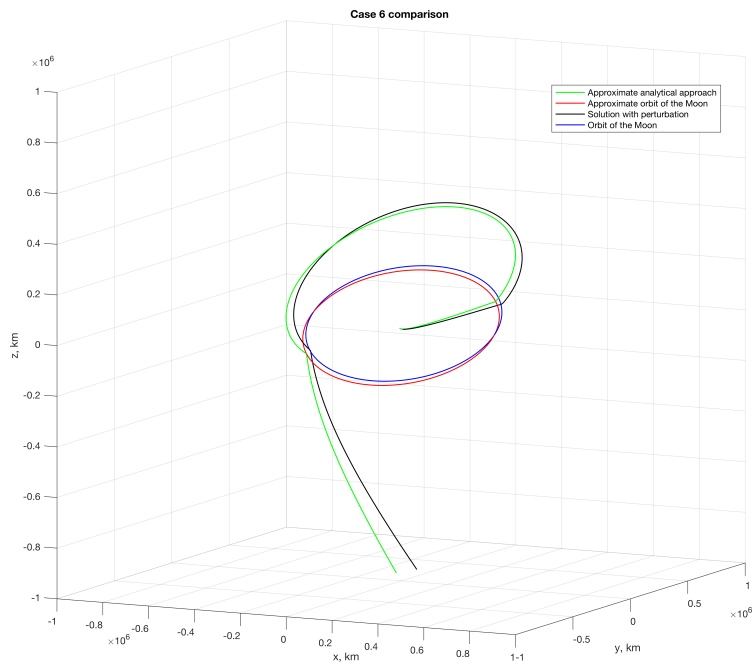


Figure 6.10: Comparison between exact and approximate solution, Case 6

## Chapter 7

# Conclusions

In this chapter, we will find a summary of all the fundamental concepts that describe all the system, already analyzed in the previous chapters.

To begin, we can underline the importance of the two flybys and the usefulness of each one. As well described, the two flybys happen after around 180 degrees because we have treated the backflip transfer. It is extremely important to notice that:

- after the first flyby, the semi-major axis decreases. All this means a slight decrease in orbital energy. Although there is this energy loss, the first flyby it is necessary to adjust the inclination: for example, as visible in Table 5.6, the inclination passes from 0.5 radians (about 28.5 degrees) to 1.78 radians (more than 100 degrees);
- the second one instead, keeps about constant the inclination and increases significantly the energy.

Although the main goal is to increase the final energy, the first flyby, that instead reduces it, is necessary to achieve the right trajectory and the desired escape conditions.

The energy values in Chapter 5 and 6 are, like all other values, dimensionless. For example, talking about the magnitude of energy of case 0, value has been increased from 0,00217 to 0,00758, with an increase of 250%. In another case, the increase reaches about 750%.

At the flybys, the S/C passes very close to the Moon. In particular the shortest distances are: for the first one, case 6, altitude of only 235 km while, for the second one, the closest is reached at case 4, with 334 km.

Another important aspect to take into account is the difference of the two model used in this document. The comparison between exact and approximated solutions shows that the results obtained through the analytical model are quite good solely for a preliminary analysis not too in-depth. It provides you the whole trajectory with a fair accuracy and the final desired shape. It provides also dates, times, positions and velocities components. As already widely underlined, positions of S/C and Moon are not exact due to the hypothesis on which the model is based. However, a good approximation is ensured. In general, this solution is only used as tentative solution for more accurate models: these approximate solutions are necessary to achieve easily convergence in the more complex models.

Even if this model has extremely simplified hypothesis, is important to notice that the relative positions between spacecraft and Moon, at both flybys, are kept. This is a key point to maintain the whole trajectory with the same shape.

Examining now the results, different considerations can be made. Talking about dates, as in Table 5.1, all the escape dates are in June 2022, while the departure takes place around April, same year. So the journey will last for about 2 months (on average 53 days). Most of this time is spent from one flyby to the other: this leg lasts for about 40 days, while from the second flyby to the escape it takes about a week. The longest leg, is characterized by an elliptical trajectory with a very high apogee (between  $9 \cdot 10^5$  and  $1 \cdot 10^6$  km).

Depending on the escape date, the trajectory in its entirety maintains almost constant the orbital parameters. Only change the angular positions at which the Moon is encountered because different times mean different Moon's positions along its orbit (increased escape date corresponds to a trajectory slightly rotated forward, counterclockwise). Analyzing Table 6.7 and Table 6.9, it can be noted that among the three cases, first flyby happens 2 days apart from each case. Remembering that Moon completes its orbit on average on 27 days, two days correspond to about 24 degrees. This angle is exactly the angular difference between Moon (and so S/C) position at the first flyby between one case to another.

That was the case of different escape dates. On the other hand, when the  $V_\infty$  is changed, it can be noted that an increase of 0.1 km/s connotes a reduction in the escape mass of only 18kg (0.2 %). Obviously, decreases also the time needed to reach the boundary of Earth's SOI.

# Glossary

- $\beta$ : Misalignment angle between the velocity directions at infinity and at the escape;  
 $\gamma_\infty$ : Flight path angle at escape;  
 $\delta$ : Angle of rotation of the velocity at both flybys;  
 $\varepsilon$ : Energy of an orbit;  
 $\eta$ : Reflectivity of the external surface of the S/C;  
 $\vartheta$ : Right ascension;  
 $\mu_E$ : Standard gravitational parameter of the Earth (398600.4415 [km<sup>3</sup>s<sup>-2</sup>]);  
 $\mu_M$ : Standard gravitational parameter of the Moon (4902.8011 [km<sup>3</sup>s<sup>-2</sup>]);  
 $\mu_S$ : Standard gravitational parameter of the Sun (1.32712440018·10<sup>11</sup> [km<sup>3</sup>s<sup>-2</sup>]);  
 $\gamma_\infty$ : Flight path angle at escape;  
 $\nu_\infty$ : True anomaly at escape;  
 $\nu_{fb}$ : True anomaly at flyby;  
 $\Phi$ : True anomaly of the asymptote;  
 $\varphi$ : Declination;
- a**: Semi-major axis;  
**a<sub>J</sub>**: Perturbation due to the Earth asphericity;  
**a<sub>lsg</sub>**: Perturbation due to the luni-solar gravity;  
**a<sub>P</sub>**: Perturbing acceleration;  
**a<sub>srrp</sub>**: Perturbation due to the solar radiation pressure;  
**ARM**: Asteroid Redirect Mission;  
**ARRM**: Asteroid Retrieval Robotic Mission;  
**ARU**: Asteroid Retrieval and Utilization;  
**AU**: Astronomical unit;  
**BVP**: Boundary value problem;  
**C3**: Hyperbolic escape energy;  
**C<sub>mn</sub>** & **S<sub>mn</sub>**: Spherical harmonic coefficients;  
 **$\bar{d}r_1$** : Position with respect to the Moon, at the first flyby;  
**e**: Eccentricity;  
**FB1**: First flyby;  
**FB2**: Second flyby;  
**incl**: Inclination;  
**IVP**: Initial value problem;  
**LGA**: Lunar gravity assist;

**$L_s$** : Total power radiated by the Sun;  
**M–M**: Moon to Moon leg;  
 **$m_u$** : Useful mass;  
 **$m_\infty$** : Useful escape mass;  
 **$m_d$** : Stage dry mass;  
 **$m_{PAF}$** : Payload attach fitting mass;  
**ODE**: Ordinary Differential Equation;  
 **$P_{mn}(\sin\varphi)$** : The associated Legendre functions;  
 **$r_M$** : Radius of Moon’s circular orbit;  
 **$r_p$** : Radius of the circular parking orbit;  
**RA**: Right ascension;  
**S/C**: Spacecraft;  
**SOI**: Sphere of influence;  
**TA**: True anomaly;  
 **$\Delta V$** : Change in velocity;  
 **$V_E$** : Circular velocity of the Earth around the Sun;  
 **$V_{H1}$** : Speed of the space vehicle on the Hohmann transfer ellipse, relative to the Sun;  
 **$\bar{V}_{M1}$** : Moon’s velocity during the first flyby;  
 **$V_P$** : Velocity at the perigee radius  $r_p$  of the departure hyperbola;  
 **$V_{PO}$** : Velocity of the circular parking orbit;  
 **$V_\infty$** : Hyperbolic escape energy;  
 **$\bar{V}_{\infty 1-}$** : Velocity before the first flyby;  
 **$\bar{V}_{\infty 1+}$** : Velocity after the first flyby;  
 **$V_1$** : Circular orbital speed of planet 1, relative to the Sun;  
 **$\bar{V}_{1-}$** : Spacecraft’s velocity before the first flyby;  
 **$\bar{V}_{1+}$** : Spacecraft’s velocity after the first flyby;  
 **$\bar{V}_r$** : Spacecraft’s radial velocity;  
 **$\bar{V}_\perp$** : Spacecraft’s tangential velocity;  
 **$(x_b, y_b, z_b)$** : Position of Sun ( $b=s$ ) or Moon ( $b=l$ ) with respect to the Earth;  
**w**: Argument of periapsis.

# Bibliography

- [1] Lorenzo Casalino and Gregory Lantoine. "Design of Lunar-GravityAssisted Escape Maneuvres". In: 2017 AAS/AIAA Astrodynamics Specialist Conference. AAS/AIAA. Aug. 22, 2017.
- [2] Colasurdo, Guido, and Lorenzo Casalino. "Indirect methods for the optimization of spacecraft trajectories." Modeling and Optimization in Space Engineering. Springer, New York, NY, 2012. 141-158.
- [3] Ceriotti, Matteo. "Global optimization of multiple gravity assist trajectories". Diss. University of Glasgow, 2010.
- [4] Curtis, Howard D. "Orbital mechanics for engineering students". Butterworth-Heinemann, 2013.
- [5] Simeoni, F., Casalino, L., Zavoli, A., and Colasurdo, G. "Indirect optimization of satellite deployment into a highly elliptic orbit". International Journal of Aerospace Engineering, 2012.
- [6] Colasurdo, Guido, and Lorenzo Casalino. "Indirect methods for the optimization of spacecraft trajectories." Modeling and Optimization in Space Engineering. Springer, New York, NY, 2012. 141-158.
- [7] Wakker, Karel F. "Fundamentals of astrodynamics." (2015).
- [8] Papkov, O. V. Multiple gravity assist interplanetary trajectories. Routledge, 2017.
- [9] [https://en.wikipedia.org/wiki/Interplanetary\\_mission](https://en.wikipedia.org/wiki/Interplanetary_mission)
- [10] [https://en.wikipedia.org/wiki/Sphere\\_of\\_influence\\_\(astrodynamics\)](https://en.wikipedia.org/wiki/Sphere_of_influence_(astrodynamics))
- [11] <http://ssd.jpl.nasa.gov/?planetephexport,2011>
- [12] <https://www.nasa.gov/content/what-is-nasa-s-asteroid-redirect-mission>
- [13] [https://en.wikipedia.org/wiki/Asteroid\\_Redirect\\_Mission](https://en.wikipedia.org/wiki/Asteroid_Redirect_Mission)
- [14] [https://en.wikipedia.org/wiki/\(341843\)\\_2008\\_EV5](https://en.wikipedia.org/wiki/(341843)_2008_EV5)
- [15] <https://echo.jpl.nasa.gov/asteroids/2008EV5/2008ev5.html>
- [16] <https://ssd.jpl.nasa.gov/?horizons>